Nonreciprocal signal routing in an active quantum network

A. Metelmann and H. E. Türeci

Department of Electrical Engineering, Princeton University, Princeton, New Jersey 08544, USA

As superconductor quantum technologies are moving towards large-scale integrated circuits, a robust and flexible approach to routing photons at the quantum level becomes a critical problem. Active circuits, which contain parametrically driven elements selectively embedded in the circuit, offer a viable solution. Here, we present a general strategy for routing nonreciprocally quantum signals between two sites of a given lattice of oscillators, implementable with existing superconducting circuit components. Our approach makes use of a dual lattice of overdamped oscillators linking the nodes of the main lattice. Solutions for spatially selective driving of the lattice elements can be found, which optimally balance coherent and dissipative hopping of microwave photons to nonreciprocally route signals between two given nodes. In certain lattices these optimal solutions are obtained at the exceptional point of the dynamical matrix of the network. We also demonstrate that signal and noise transmission characteristics can be separately optimized.

I. INTRODUCTION

The goal to achieve accurate control over propagation of electromagnetic waves has motivated a great deal of research in photonics. Experimental progress in photonic crystals and metamaterials has matured to a degree that nanofabricated semiconductor and metallic optical structures provide fabrics for guiding and storing light that allow highly accurate control over desired metrics. The recognition that a fundamental limitation is imposed due to backscattering of light from unavoidable fabrication imperfections has driven the search for a new generation of optical materials that benefit from the imposition of electromagnetic nonreciprocity, without a reliance on magneto-optical effects. A number of effective strategies have been devised to achieve such nonreciprocity. One strategy relies on the implementation of a direction-dependent phase in a lattice of resonators with time-modulated coupling strength [1]. The idea here is the generation of a synthetic gauge field that gives rise to a band structure eliciting topologically protected one-way edge states [1–6]. Another approach relies on the special properties of an effective non-Hermitian generator for light propagation [7–11].

Here we study the quantum transport of electromagnetic excitations in a lattice that is subject to parametric driving. We show how control over the flow of light can be exercised by optimizing the spatial pattern of parametric driving (amplitude, phase, and frequency). The performance metrics we choose here relate to nonreciprocal propagation between two ports connected to the lattice; see Fig. 1. The nonreciprocal propagation in the active lattice is generated through a quantum bath engineering approach. Interference between coherent and dissipative hopping among primary nodes of the active lattice is specifically engineered to destructively cancel all other propagation paths than the desired one. The physics of the unit cell of the lattices we consider here was introduced in Refs. [12,13]. The dissipative component of hopping is engineered through an auxiliary node ("link oscillator") that

is deliberately chosen to be lossier than the primary nodes of the lattice. The lattice of parametrically driven oscillators, in the limit of vanishing coupling to link oscillators, possesses a band structure that has *no* topologically nontrivial properties. Nonreciprocal propagation arises here purely due to finite loss, in contrast to earlier work on nonreciprocal propagation that relies on the existence of chiral edge states of an associated bulk that has a topologically nontrivial band structure [1,14].
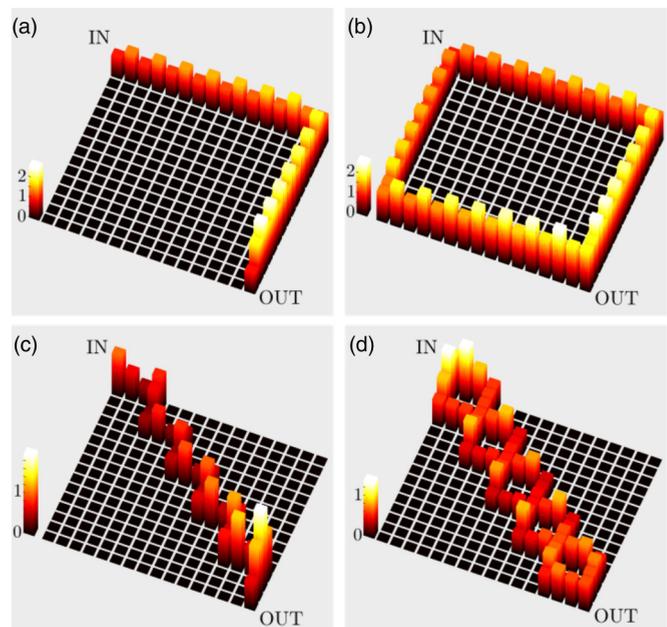
FIG. 1. Directional propagation in an oscillator lattice with 256 sites. An input signal is injected on the upper left corner and propagates along a predesigned path to the output waveguide attached to the lower right oscillator. Depicted is the averaged steady-state amplitude of each oscillator.
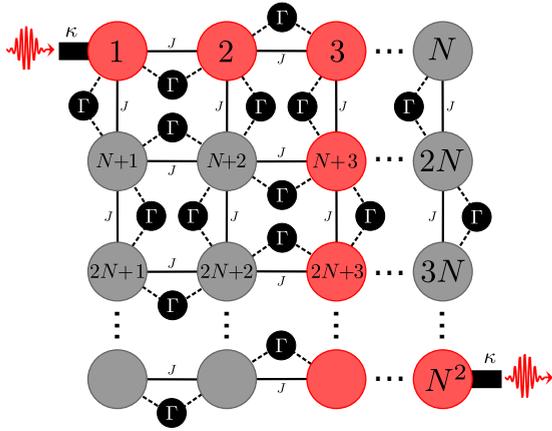
FIG. 2. Illustration of the active lattice. Each oscillator of the N^2 lattice is directly coupled to its neighboring oscillators (solid lines). For simplicity we assume here uniform coupling strengths $G_{ij}e^{i\phi_{ij}} \equiv J$. Additionally, each oscillator pair is indirectly coupled via link oscillators (black circles), giving rise to an incoherent indirect exchange at the rate Γ. Oscillators 1 and N^2 are coupled to external waveguides with coupling strength κ. The red circles denote a possible propagation path through the lattice if a signal is injected on oscillator 1 and transmitted to oscillator N^2.

Quantum transport in a parametrically driven lattice in principle requires the solution of the many-body problem of an array of driven dissipative nonlinear oscillators. We show that this problem in appropriate operation regimes can be reduced to a set of linear Heisenberg-Langevin equations governed by a non-Hermitian matrix below the parametric instability threshold. The parameters of this non-Hermitian matrix are the drive amplitudes, frequencies, and phases, providing a flexible active fabric for propagation of electromagnetic excitations that is dynamically tunable. The optimization problem then is shown to be generally governed by special points in the parameter space where the dynamical non-Hermitian matrix becomes singular. Such points are referred to as "exceptional points" (EPs) and have been discussed extensively in the context of wave propagation and lasing, in particular in connection with $\mathcal{PT}$-symmetry breaking [7–11]. The presented problem and the associated analysis requires consideration of quantum fluctuations, noise, and quantum nonlinearities in the presence of such EPs.

We propose a realization of such an active lattice using components that are readily available in superconducting circuits. The unit cell of the active lattice discussed here (containing three oscillators) has been studied theoretically [12,15] and has been already realized experimentally in superconducting circuits and optomechanical systems with compact and scalable components [16–20]. For these realizations focusing on circulator-like geometries signal routing is not a concern (or definable); such a possibility emerges in a lattice as discussed in this work.

II. THE ACTIVE-LATTICE EFFECTIVE HAMILTONIAN

We consider a lattice of oscillators (Fig. 2) where the exchange of excitations between two nodes d_i and d_j takes place via two processes: a direct exchange (amplitude $G_{ij}e^{-i\phi_{ij}}$) and an indirect exchange via a link oscillator $\hat{d}_{ij}$ (amplitudes $G_{i;ij}$,

$G_{j;ij}$). The dynamics of such a system is governed by the effective Hamiltonian

$$\hat{\mathcal{H}} = \sum_{\langle i,j \rangle} G_{ij}\,\hat{d}_i^\dagger \hat{d}_j e^{-i\phi_{ij}} + G_{i;ij}\,\hat{d}_i^\dagger \hat{d}_{ij} + G_{j;ij}\,\hat{d}_j^\dagger \hat{d}_{ij} + \text{H.c.}$$

(1)

Here, $\langle i,j \rangle$ denotes nearest-neighbor nodes and the indices i and j run over integers $1,\ldots,N^2$, from left to right and top to bottom. The hopping elements G_{ij}, $G_{i;ij}$, and $G_{j;ij}$ are assumed to be real-valued. A crucial element here is the tunable nonzero phase ϕ_{ij}. This lattice model with adjustable parameters G and ϕ can be realized through parametric processes, which will be discussed in more detail in the implementation section. We furthermore specify that each link oscillator $\hat{d}_{ij}$ is coupled to a reservoir that gives rise to dissipation at rate κ_{ij} and is subject to the associated noise. The goal is to design the parameters G_{ij}, $G_{i;ij}$, $G_{j;ij}$, and ϕ_{ij} to nonreciprocally route an excitation injected from the site $i = 1$ to the site $i = N^2$, where the signal is to be collected, as shown in Fig. 2.

We also consider amplification of the injected signal, which can be implemented by reconfiguring the parametric interactions on a given link oscillator. This leads to the following interaction between the link and the node oscillators:

$$\hat{\mathcal{H}}_{\text{PA}} = \sum_{\langle i,j \rangle} G_{ij}\,\hat{d}_i^\dagger \hat{d}_j e^{-i\phi_{ij}} + G_{i;ij}\,\hat{d}_i^\dagger \hat{d}_{ij}^\dagger + G_{j;ij}\,\hat{d}_j^\dagger \hat{d}_{ij}^\dagger + \text{H.c.},$$

(2)

which can be optimized to yield one-way propagation with a tunable gain from oscillator j to $j + 1$.

III. ONE-WAY TRANSPORT BETWEEN TWO NODES

We first discuss the basic building block of the proposed active lattice, namely the implementation of one-way transport between *two* isolated nodes, $i \rightarrow j$. We assume in what follows that κ_{ij}, the dissipation acting on the link oscillator ij, is the dominant loss channel in the system. Using a Heisenberg-Langevin approach (see Appendix A), the conditions for one-way propagation can be extracted by considering the dynamics of expectation values $\bar{d}_n \equiv \langle \hat{d}_n \rangle$ and adiabatically eliminating the link oscillator:

$$\dot{\bar{d}}_i = -\frac{\Gamma_{i;ij}}{2}\bar{d}_i - \left[iG_{ij}e^{-i\phi_{ij}} + \frac{\sqrt{\Gamma_{i;ij}\Gamma_{j;ij}}}{2} \right]\bar{d}_j,$$

$$\dot{\bar{d}}_j = -\frac{\Gamma_{j;ij}}{2}\bar{d}_j - \left[iG_{ij}e^{+i\phi_{ij}} + \frac{\sqrt{\Gamma_{i;ij}\Gamma_{j;ij}}}{2} \right]\bar{d}_i. \quad (3)$$

Here $\Gamma_{n;ij} = 4G_{n;ij}^2/\kappa_{ij}, (n \in i, j)$. We aim for the situation where the oscillator j is driven by the oscillator i but not vice versa. This can be achieved through balancing the effective dissipative hopping term generated by the integration out of the link oscillator, the second term in the square brackets, with the unitary hopping term, given by the first term. The balancing conditions become

$$\phi_{ij} = -\frac{\pi}{2} \quad \text{and} \quad G_{ij} = \frac{\sqrt{\Gamma_{i;ij}\Gamma_{j;ij}}}{2}. \quad (4)$$
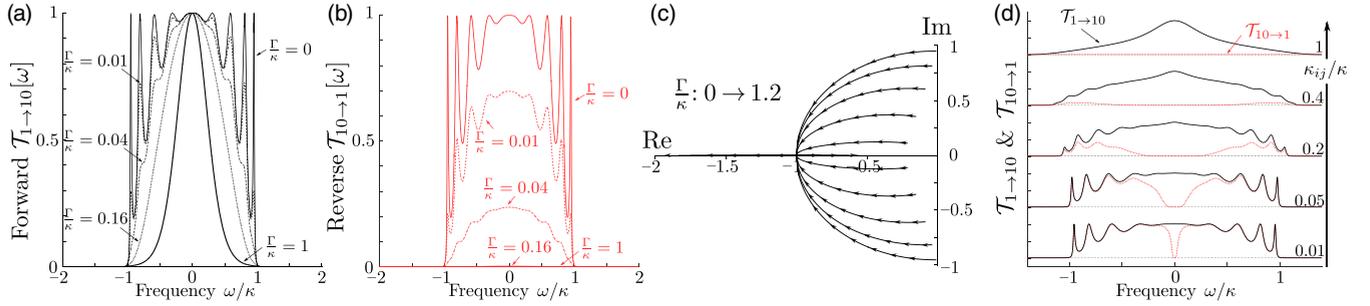
FIG. 3. Transmission properties and eigenvalues for a chain of $N = 10$ oscillators with fixed coherent hopping strength $|J| = \kappa/2$. (a), (b) Forward and backward transmission for various values of Γ/κ. The transmission window is determined by the coherent hopping strength; i.e., transmission in both directions is possible in the frequency range $\Delta\omega = 4|J|$. Once the directionality condition $\Gamma/\kappa = 1$ is met, the reverse transmission vanishes. (c) Eigenvalues of the dynamical matrix for various values of Γ/κ. Below the exceptional point, i.e., $\Gamma/\kappa < 1$, the system shows underdamped oscillations. The point of directionality at $\Gamma/\kappa = 1$ coincides with an exceptional point, where all eigenvalues are degenerate and real. For $\Gamma/\kappa > 1$ the eigenvalues are purely real, implying overdamped dynamics. (d) Forward and backward transmission for fixed directionality condition, as the damping rate of the link oscillators κ_{ij} is varied. The bandwidth in which nonreciprocal transmission is possible is on the order of $2\kappa_{ij}$. It is seen that the reverse transmission gets suppressed even for modest values of κ_{ij}.

This condition provides a *manifestly* directional coupling for excitations (at the equation of motion level, j is coupled to i but not vice versa).

This mechanism for nonreciprocal transport between two oscillators through the balancing of dissipative and coherent hopping was first proposed in Ref. [12]. Recent experimental work in three-mode systems has demonstrated superconducting circulators and directional amplifiers operating close to the standard quantum limit [16,18]. These experiments essentially implement conditions similar to the one stated in Eq. (4), as has been also found in Ref. [15]. Nonreciprocal signal propagation via a dissipation-based approach was recently implemented in an optomechanical setup as well [17]. The generalization of these considerations to an $N \times N$ lattice requires the satisfaction of further conditions while providing additional functionalities, which we discuss below.

IV. NONRECIPROCAL SIGNAL PROPAGATION

The evaluation of transport characteristics requires the system to be opened up to the environment. Besides that, we aim to design the finite dissipation on the link oscillators to control the transport of excitations. Therefore the active-lattice dynamics has to be addressed through an open-system approach. This regime should be contrasted to earlier work in lattices subject to artificial gauge fields [1,21–26] where dissipation is generally expected to be minimized and does not play a critical role. In the latter case, directional propagation is possible due to topologically protected edge states and can be described through Hamiltonian dynamics. Because the optimal conditions we find sensitively depend on the lattice dimensionality and geometry, we first discuss the case of a one-dimensional chain.

We begin by illustrating the conditions for nonreciprocal transport in a chain of N oscillators. Coupling the input (d_1) and output (d_N) oscillators to external waveguides, while giving rise to an adjustable coupling loss κ (assumed equal for both ports without loss of generality), allows us to study signals entering and leaving the chain. For simplicity, we assume uniform couplings $G_{ij}e^{i\phi_{ij}} \equiv J$ and $\Gamma \equiv 4G_{n;ij}/\kappa_{ij}, (n \in i, j)$.

The condition Eq. (4) is then $J = -i\Gamma/2$, resulting in the decoupling of the jth oscillator from the $j + 1$th oscillator. This decoupling leads to a situation where an oscillator in the chain is driven by its left neighbor, but never from any higher element in the chain; i.e., the stationary solution of each oscillator becomes $\bar{d}_j = -\bar{d}_{j-1}$. By using standard input-output theory [27], $\hat{d}_{j,\text{out}} = \hat{d}_{j,\text{in}} + \sqrt{\kappa}\hat{d}_j$, the scattering between the input and output ports is described by a 2×2 scattering matrix $\mathbf{s}[\omega]$:

$$\mathbf{D}_{\text{out}}[\omega] = \mathbf{s}[\omega]\,\mathbf{D}_{\text{in}}[\omega] + \hat{\vec{\xi}}[\omega], \quad \mathbf{D}[\omega] = (\hat{d}_1[\omega], \hat{d}_N[\omega])^T.$$

(5)

Here, $\hat{\vec{\xi}}[\omega]$ accounts for noise incident on the oscillators from the waveguides and the zero frequency scattering matrix is

$$\mathbf{s}[0] = \begin{pmatrix} \frac{\Gamma-\kappa}{\kappa+\Gamma} & 0 \\ \frac{(-1)^N 4\kappa\Gamma}{(\kappa+\Gamma)^2} & \frac{\Gamma-\kappa}{\kappa+\Gamma} \end{pmatrix} \overset{\Gamma \equiv \kappa}{=} \begin{pmatrix} 0 & 0 \\ (-1)^N & 0 \end{pmatrix}.$$

(6)

Thus by applying the impedance matching condition $\Gamma = \kappa$ in the second step, we realize the scattering matrix of a perfect isolator. No input on oscillator N will ever show up at the output of oscillator 1, while any input on oscillator 1 will be perfectly transmitted to oscillator N, i.e., $|s_{21}| = 1$. Interestingly, the impedance matching condition requires that κ, the coupling to input and output waveguides, be the same order as the hopping strength $|J|$ [$= \Gamma/2$ to satisfy Eq. (4)]. We note that this condition is not necessary for nonreciprocity, but it prevents unwanted back-reflection of an injected signal.

Next we consider the transmission away from resonance. In the absence of incoherent hopping via the link oscillators, $\Gamma = 0$, forward and reverse transmission display N resonance peaks and are identical as required by reciprocity [see Figs. 3(a) and 3(b) for $\Gamma/\kappa = 0$]. We note that the operation point of choice requires that the chain be in the low-finesse regime ($|J| = \kappa/2$); thus not all resonances (in particular those near the center of the band) are well resolved. As Γ is turned on, forward transmission peaks in Fig. 3(a) gradually smear out. When the directionality matching condition $\Gamma = 2|J| = \kappa$ is satisfied the entire band originally of width $4J$ collapses to a single Lorentzian peak with a bandwidth on the order of

$\kappa/2$. Simultaneously reverse transmission [Fig. 3(b)] is seen to vanish completely within the band.

The analysis of the spectrum of the dynamical matrix $\mathcal{L}$, defined by $\dot{\bar{\mathbf{d}}} = \mathcal{L}\,\bar{\mathbf{d}}$ where $\bar{\mathbf{d}} = [\langle\hat{d}_1\rangle\langle\hat{d}_2\rangle\cdots\langle\hat{d}_N\rangle]^T$, reveals another interesting aspect of the nonreciprocity condition found. Due to the coupling to the waveguides and the dissipative link oscillators, $\mathcal{L}$ is a non-Hermitian matrix and its eigenvalues $\mathcal{L}\,\mathbf{v}_n = \varepsilon_n\mathbf{v}_n$ are generally complex-valued. For $\Gamma = 0$, the system dynamics is governed by N complex eigenvalues whose real and imaginary parts give the damping rates and the associated resonance frequencies, respectively, of Bloch modes of an open tight-binding oscillator chain (for vanishing waveguide coupling $\kappa \to 0$ the eigenvalues would be purely imaginary $\varepsilon_n = 2i|J|\cos[n\pi/(N+1)]$ implying undamped, coherent dynamics). As Γ approaches the nonreciprocity condition, the eigenvalues collapse to an N-fold-degenerate *purely real* eigenvalue given by $\varepsilon_n = -\kappa$ [Fig. 3(c)], implying overdamped dynamics. The inspection of eigenvectors reveals that all eigenvectors are degenerate as well; hence the nonreciprocity condition found coincides with an exceptional point. The role of such special degeneracies and their connection to unusual dynamical regimes have recently attracted a lot of interest in coupled optical cavities operating in the classical regime [9–11,28–30].

A remaining important parameter is the damping rate κ_{ij} of each link oscillator; it determines the frequency band over which the transmission can be rendered nonreciprocal. To sufficiently suppress the reverse transmission requires $\kappa_{ij}/\kappa > 1$ [Fig. 3(d)]. The directionality bandwidth is on the order of $\Delta_d = 2\kappa_{ij}$; i.e., a detuning of $\Delta_d/2$ from resonance corresponds to a 3 dB isolation between forward and reverse transmission [31].

V. THE 2D SYSTEM

The consideration of nonreciprocal transmission in a two-dimensional lattice introduces an additional aspect. There is a large degree of freedom in designing nonreciprocal transmission between two ports attached to such a lattice, posing in principle a difficult optimization problem. This large optimization space also harbors a unique opportunity to route excitations nonreciprocally through a path that is dynamically reconfigurable. The optimization space we consider consists of the choice of link variables $\{\Gamma_{ij}, \phi_{ij}\}$ for dissipative hopping. Additionally, amplification stages via the interaction Eq. (2) will be inserted between select nodes $\{\widetilde{\Gamma}_{ij}, \tilde{\phi}_{ij}\}$. We aim for flexibility in how we choose to propagate through the lattice while keeping a simple pattern for the oscillator couplings.

We first analyze a configuration that allows the nonreciprocal routing of the excitation around one edge of the lattice, as shown in Fig. 1(a). An analytic solution can be obtained for a configuration with uniform dissipative coupling strength $\Gamma_{ij} = \Gamma$ on all links ("dissipative links") and choosing the pattern of phases $\phi_{ij} = \pm\pi/2$ as shown in Fig. 4 for the example of a lattice of 16 oscillators. In addition we insert an amplifying link at every second link along the designated edge of propagation (except at the corners) and denote the effective coupling strength of two neighbors at these stages as $\widetilde{\Gamma}$. The latter is a measure of how strongly we amplify the signal on its way through that link. Impedance matching and nonreciprocal
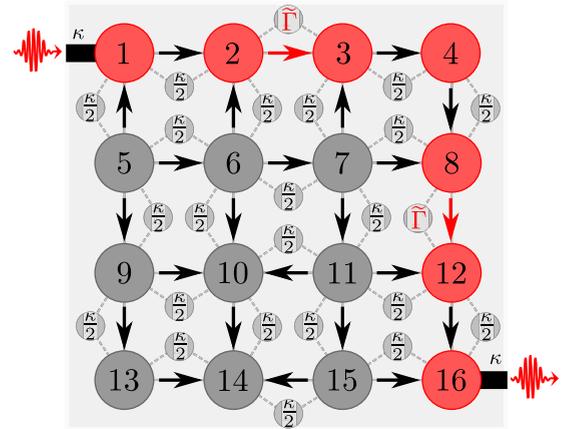
FIG. 4. Parametrization for nonreciprocal propagation along one edge in a 16-oscillator lattice. We implement two amplification stages on the upper and the left edge with $\Gamma_{23} = \Gamma_{812} = \widetilde{\Gamma}$ and $\tilde{\phi}_{23} = \tilde{\phi}_{812} = \pi/2$. The remaining couplings are uniformly chosen to be $\Gamma = 2|J| = \kappa/2$. The phases depend on the propagation direction as indicated by the black arrows; we have $\phi_{ij} = -\pi/2$ for $\to, \downarrow$ and $\phi_{ij} = +\pi/2$ for $\leftarrow, \uparrow$. In principle, only the phases and couplings of the signal-carrying oscillators (red circles) and their nearest neighbors have to be fixed. The remaining oscillators do not affect the transmission properties of the lattice.

propagation is ensured for the choice $\Gamma = 2|J| = \kappa/2$. For these conditions, forward transmission is given by

$$\mathcal{T}_{1\to N^2} = \frac{1}{4}\left[\frac{2\widetilde{\Gamma}\kappa}{(\kappa - \widetilde{\Gamma})^2}\right]^{2N-4}, \tag{7}$$

from which we infer that stability requires $\widetilde{\Gamma} < \kappa$. Figure 5(c) (i) depicts the transmission as a function of $\widetilde{\Gamma}$ for various lattice sizes N, showing that considerable signal amplification can be attained while staying away from the instability condition $\widetilde{\Gamma} = \kappa$. To transfer a signal successfully through the lattice, the implementation of the amplification stages is crucial. Without the latter, the propagation is still nonreciprocal and over the edge but the signal amplitude decays due to induced local damping; cf. Fig. 5(a) graph (vi) vs (ix).

VI. NOISE CHARACTERISTICS

Noise at the output port can be characterized by the symmetrized noise spectral density $\bar{S}_{N^2,\text{out}}[\omega] = \frac{1}{2}\int\frac{d\Omega}{2\pi}\langle\{\hat{d}_{N^2,\text{out}}[\omega], \hat{d}^\dagger_{N^2,\text{out}}[\Omega]\}\rangle$ which can be evaluated using input-output theory. For example, taking the configuration discussed in the previous section (e.g., Fig. 4), the added noise referred back to the input yields

$$\bar{n}_{\text{add}} = \frac{\bar{S}_{N^2,\text{out}}[0]}{\mathcal{T}_{1\to N^2}} - \left(\bar{n}^T_{d_1} + \frac{1}{2}\right) \simeq 7\left(\bar{n}^T_{\text{link}} + \frac{1}{2}\right) \tag{8}$$

for large gain, i.e., $\widetilde{\Gamma}/\kappa \to 1$, and equal bath temperatures for all link oscillators; see Appendix C 2 for details of the derivation. Thus for zero temperature and large gain, the active lattice adds a minimum noise of 3.5 quanta to the signal. Inspection of Fig. 5(c) (i) reveals that this large-gain limit for noise has an asymptote that is independent of the size of the lattice N. Crucially, we find that the noise characteristics at the output
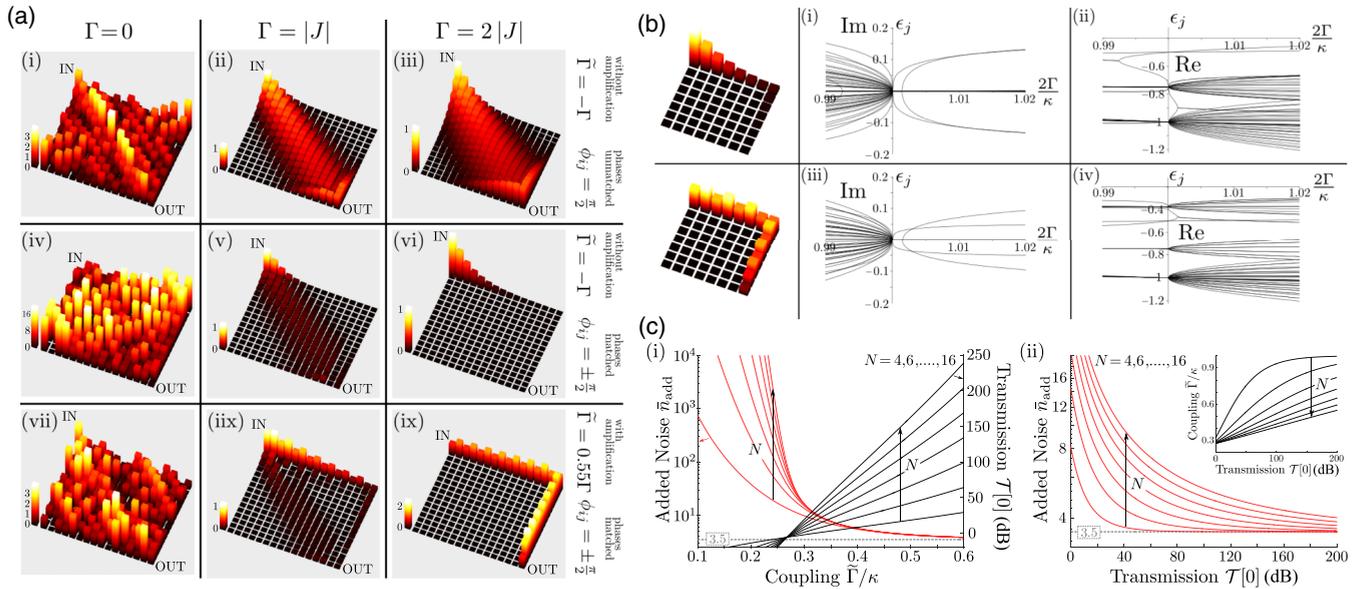
FIG. 5. Characteristics of nonreciprocal signal propagation along one edge. (a) Averaged steady-state amplitude of each oscillator in a lattice of 256 cavities. The coherent hopping strength is fixed, i.e., $|J| = \kappa/4$ and $|J| = 0.55 \times \kappa/4$ for the amplification links if applicable, while the dissipative coupling strength is increased from the left to right column. Once the directionality conditions are matched, i.e., graphs (vi) and (ix), only the edge cavities have a finite occupation. However, to have a transmission close to unity, amplification stages have to be implemented. (b) Eigenvalues for an $N = 8$ oscillator lattice without and with amplification. The coherent hopping strength is set to $|J| = \kappa/4$ and the dissipative rate Γ is varied. The dynamics at the point of directionality is described by purely real eigenvalues. Note, this fact is independent of the chosen propagation path and the lattice size; for details see Appendix C. (c) Transmission and added noise for propagation over one edge. By increasing $\tilde{\Gamma}/\kappa$ the signal gets amplified, while the added noise is suppressed. For $\tilde{\Gamma}/\kappa \to 1$ the transmission diverges and the noise reaches its minimal value of 3.5. In panel (c) (i) the suppression of the added noise is rather independent of the lattice size. The reason therefore is that a larger lattice size involves more amplification stages; thus, a larger coupling strength $\tilde{\Gamma}$ results in a higher gain value. Comparing the added noise for various N and fixed transmission value we see that a larger lattice size requires a larger amount of gain to come close to the quantum limit; cf. graph (c) (ii).

largely depend on the placement of the first amplification stages. This is also the reason behind the observed insensitivity of the noise to the lattice size. The noise contribution added to the signal before an amplification stage is entered sets the minimum of the added noise. This is simple to understand: the noise added before the amplification stage gets amplified in the same manner as the signal and cannot be suppressed in any way.

For the general case of propagation along one edge in a lattice of N^2 oscillators the first amplification stage is placed between the node oscillators 2 and 3. Hence, we can reduce the noise analysis to the upper left corner in the lattice, i.e., to the node oscillators $1, 2, N + 1$, and $N + 2$ and the link oscillators surrounding them. We assume that each oscillator pair couples with the same strength to their respective link oscillator, i.e., we set $\Gamma_{n,ij} \equiv \Gamma_{i,j}$, and assume that the corresponding directionality conditions between two oscillators are met, i.e., we set $G_{ij} = \Gamma_{i,j}/2$ and adjust the phases in the desired manner. Additionally, we neglect any intrinsic losses in the node oscillators, so that the noise originates solely from the link oscillators. The noise flow between the four node oscillators and the corresponding link oscillators is depicted in Fig. 6(a). Each oscillator pair is exposed to the fluctuations of the respective link oscillator which couples them, and the noise can take multiple paths from its origin to the node oscillator 2. Crucially, while propagating the noise contributions acquire different phase shifts and can destructively interfere at the node

oscillator 2. This interference is only possible for paths taken within a closed loop involving the source link oscillator and the node oscillator 2, i.e., contributions from the blue-shaded link oscillators in Fig. 6(a). However, the noise contribution from black-shaded link oscillators in Fig. 6(a) cannot destructively interfere, as no closed loops are formed. The latter will determine the minimum of noise which is added to the signal.

Figure 6(b) depicts the individual paths taken by the noise contributions which propagate along a close loop to the node oscillator 2. For optimal propagation the couplings of the node oscillator 2 to the remaining oscillators have to be matched to their local dampings; i.e., we have to ensure that the noise contributions are transmitted to the node oscillator 2 with unity transmission. We can extract three optimal noise canceling conditions:

(i) $\Gamma_{1,2} = \kappa + \Gamma_{1,N+1},$

(ii) $\Gamma_{2,N+2} = \Gamma_{N+1,N+2} + \Gamma_{N+2,N+3} + \Gamma_{N+2,2N+2},$

(iii) $\Gamma_{N+1,2N+1} = \Gamma_{1,N+1} + \Gamma_{N+1,N+2},$ (9)

where we illustrate in Fig. 6(b) the propagation loops matching all three conditions. Taking for example the graph (i) in Fig. 6(b), the noise of the link oscillators $\hat{d}_{12,\text{in}}$ propagates via two paths to the node oscillator 2: directly and via the node oscillator 1. The effective coupling between the two oscillators is $\Gamma_{1,2}$, while the local damping of the node oscillator 1 is given as $(\Gamma_{1,2} + \kappa + \Gamma_{1,N+1})/2$. Under condition (i) the local
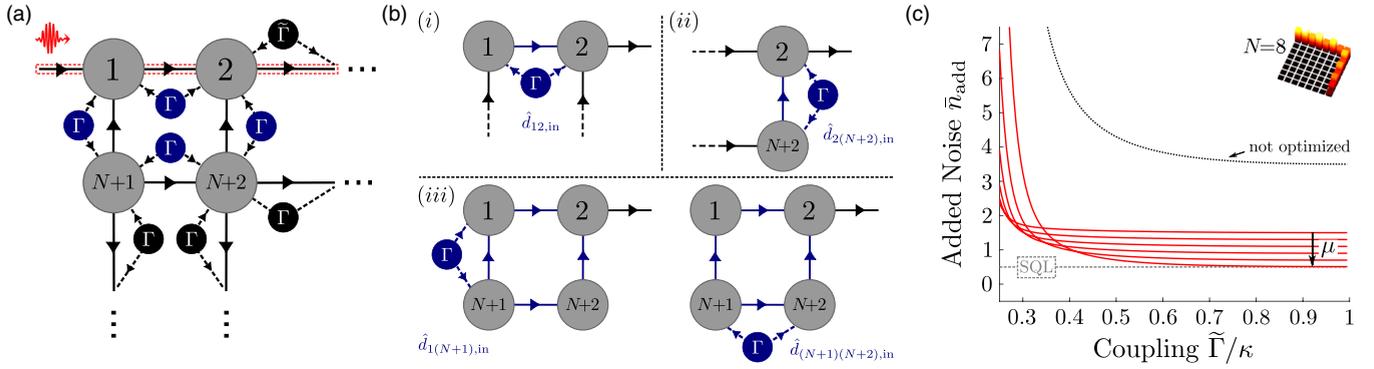
FIG. 6. Optimization of the noise properties for propagation along one edge. (a) Noise contribution and their flow when the corresponding directionality conditions are met. The red dashed area indicates the propagation of the signal injected into the node oscillator 1. Neglecting intrinsic losses in the cavities, the noise contamination originates solely from the lossy link oscillators. Crucially, the noise contributions arising from the blue-shaded link oscillators can deconstructively interfere, while the noise contributions from the black-shaded link oscillators cannot be compensated. (b) Possible interference paths in the noise flow. Under optimal conditions as given in Eq. (9) the noise contributions from the blue-shaded link oscillators are canceled. (c) Optimizing the added noise for an $N = 8$ oscillator lattice. The black-dotted line depicts the added noise without optimization, i.e., parameters setting as in Fig. 4. Parameters for the upper left 2×2 block of oscillators are $\Gamma_{2,N+2} = \Gamma_{1,N+1} = \mu\kappa/2$, $\Gamma_{N+1,N+2} = \Gamma_{N+2,N+3} = \Gamma_{N+2,2N+2} = \mu\kappa/6$, and the optimization conditions in Eq. (9) are met. For stability reasons we choose as well $\Gamma_{3,N+3} = \kappa/2 + \Gamma_{1,N+1} + \Gamma_{2,N+2}$. The remaining lattice parameters are chosen as in Fig. 5. By increasing the coupling $\widetilde{\Gamma}$ and for small factor μ the added noise drops close to the standard quantum limit (SQL) of a phase-insensitive linear amplifier. Note, the coupling for the first amplification stage between the node oscillators 2 and 3 is set to $\widetilde{\Gamma}_{\mathrm{opt}} = \widetilde{\Gamma} + \Gamma_{1,N+1} + \Gamma_{2,N+2}$ to adjust the gain factor to the remaining amplification stages.

damping and effective coupling strength coincide; hence the noise of the link oscillators $\hat{d}_{12,\mathrm{in}}$ arrives via both paths with the same amplitude at the node oscillator 2. Importantly, along the path via the node oscillator 1 a phase shift of π is acquired, and combined with condition (i) in Eq. (9) the noise deconstructively interferes at the node oscillator 2. Similar arguments hold for the noise contributions $\hat{d}_{2(N+2),\mathrm{in}}$ leading to condition (ii) in Eq. (9). However, the cancellation of the noise contribution from the two link oscillators $\hat{d}_{1(N+1),\mathrm{in}}$ and $\hat{d}_{(N+1)(N+2),\mathrm{in}}$ requires only one condition. For the case that conditions (i) and (ii) are met, the node oscillator 2 couples indirectly via its direct neighbors to the node oscillator $N + 1$ with the effective coupling strength $\Gamma_{\mathrm{eff}} = \Gamma_{1,N+1} + \Gamma_{N+1,N+2}$. This indirect coupling Γ_{eff} has then to be matched to the local damping of the node oscillator $N + 1$, resulting in condition (iii).

To determine now the minimum of added noise we calculate the symmetrized noise spectra of the node oscillator 2. Applying the optimization conditions in Eq. (9) we obtain (assuming zero temperature)

$$\bar{S}_2[0] = \frac{1}{2}\,\mathcal{G}_2'\left[1 + (\widetilde{\Gamma}_{\mathrm{opt}} + \Gamma_{1,N+1} + \Gamma_{2,N+2})\frac{1}{\kappa}\right]. \quad (10)$$

Here we denote $\widetilde{\Gamma}_{\mathrm{opt}}$ as the effective coupling between the node oscillators 2 and 3, i.e., the first amplification stage, and with the gain factor

$$\mathcal{G}_2' = \frac{4\kappa}{[\kappa + \Gamma_{1,N+1} + \Gamma_{2,N+2} - \widetilde{\Gamma}_{\mathrm{opt}}]^2}, \quad (11)$$

from which we see that for stability reasons we need $\widetilde{\Gamma}_{\mathrm{opt}} < \kappa + \Gamma_{1,N+1} + \Gamma_{2,N+2}$. Note, we consider here the intraoscillator spectra; hence the gain factor has the dimension of an inverse rate. As mentioned above, the minimum of the added noise is set by the noise contamination appearing before an

amplification stage is entered; here this corresponds to the noise added till the signal arrives at the node oscillator 2. Hence, in the regime of large gain, we can approximate the minimal added noise as

$$\bar{n}_{\mathrm{add}} \simeq \frac{\bar{S}_2[0]}{\mathcal{G}_2'} - \frac{1}{2} \simeq \frac{1}{2} + [\Gamma_{1,N+1} + \Gamma_{2,N+2}]\frac{1}{\kappa}; \quad (12)$$

hence, for $\Gamma_{1,N+1}, \Gamma_{2,N+2} \ll \kappa$ the added noise approaches the value 0.5. The latter is the expected limit as we effectively have a linear phase-insensitive amplifier, with the standard quantum limit of half a quantum. We can verify numerically that this is actually the minimal added noise for the whole lattice. In Fig. 6(c) we plot the added noise as a function of coupling strength $\widetilde{\Gamma}$, i.e., for increasing gain, and under the optimal noise cancellation conditions given in Eq. (9). We set $\Gamma_{1,N+1} = \Gamma_{2,N+2} = \mu\kappa/2$ and find that for $\mu \to 0$ the noise drops close to $1/2$. Note, depicted is the noise for a 64-oscillator lattice, but, as before, we find that the minimum of added noise is independent of the lattice size.

For the case of vanishing couplings to the second row, i.e., $\Gamma_{1,N+1} = \Gamma_{2,N+2} = 0$, the added noise in Eq. (12) is minimal and the subsystem made of oscillators 1 and 2 is effectively reduced to a 1D chain. Clearly, from a more practical perspective, 1D propagation is superior for a two-port device; i.e., deactivating all couplings in the 2D lattice except the ones along the desired propagation path will result in optimal noise performance. Moreover, a simple two-port routing device does in principle not require a 2D structure; i.e., an isolator is realized within a single unit cell of the lattice. However, multiport routers will require small lattice structures in which our findings will be of importance. In addition, for nonreciprocal propagation with gain a multiunit architecture can be advantageous, as the number of amplification stages directly contributes to the signal gain and increasing their
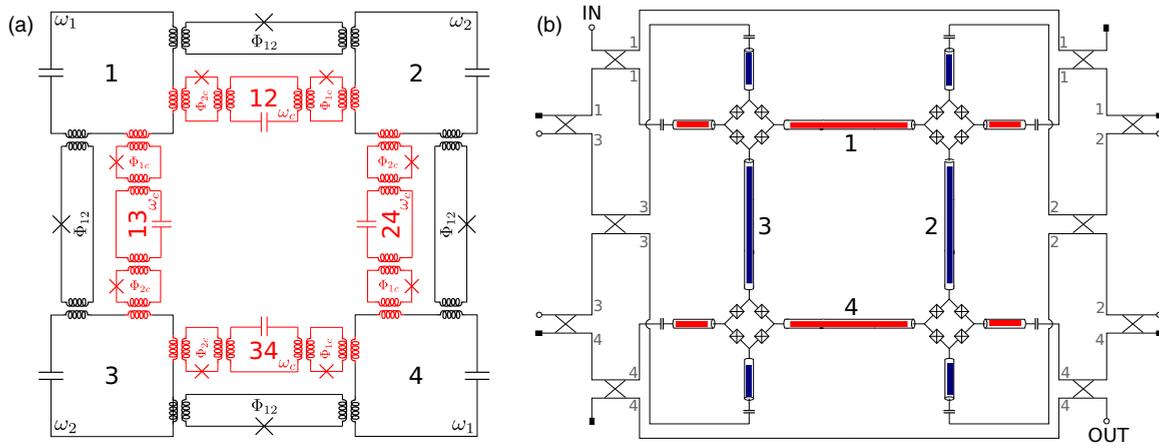
FIG. 7. Possible implementations for a 2×2 lattice in superconducting circuit architectures. (a) Circuit schematic for a lattice of LC resonators. The oscillators are pairwise coupled via tunable couplers, i.e., a loop intersected by a Josephson junction. Applying a flux Φ_{ij} to the loops realizes a tunable coupling $g_{ij}(t)$ between the oscillators. For resource efficiency we choose the link oscillator (red lines) to be degenerate in frequency (ω_c), and the node oscillators 1 (2) and 4 (3) are degenerate in frequency ω_1 (ω_2) as well. Due to these degeneracies the 12 coupler loops require only three distinct flux values (Φ_{12}, Φ_{1c}, and Φ_{2c} as denoted in the graph). (b) Example of an implementation utilizing Josephson parametric converters (JPCs), devices which realize three-wave mixing between the orthogonal modes X, Y, and Z of each JPC. For the lattice setup, the common mode Z of each JPC corresponds to the link oscillators, while the modes X and Y form the node oscillators (highlighted in red and blue). Note, in contrast to a standard JPC setup [16], this design requires that each microstrip resonator be intersected with two JRMs.

number helps in keeping the operation point of individual amplification stages away from the instability point. The design of multiport routers and reconfigurable lattice amplifiers will be a focus of future work.

VII. IMPLEMENTATION

In this section we discuss the physical implementation of the active-lattice Hamiltonian Eq. (1) with superconducting electrical circuits. We note that these effective interactions present in this Hamiltonians are linear. The implementations we discuss require the dynamic modulation of nonlinear elements with multiple tones to generate the requisite linear interaction terms in an appropriate rotating frame.

The first implementation we discuss is a lattice of LC resonators which are pairwise connected via tunable coupler loops [14,32]; see Fig. 7(a) for the example of a circuit diagram of a 2×2 lattice. Each tunable coupling loop is intersected with a single Josephson junction and inductively coupled to two oscillators. Treating the loop by an external magnetic flux allows for a tunable coupling $g(t)$ between these oscillators. This tunable coupling element between two oscillator modes $\hat{a}$ and $\hat{b}$ has been discussed [32] and implemented experimentally [14]. In these setups a pairwise interaction between the two modes can be generated, given by $\hat{\mathcal{H}} = g(t)(\hat{a} + \hat{a}^{\dagger})(\hat{b} + \hat{b}^{\dagger})$. Harmonic modulation $g(t) = G \cos(\omega_p t + \phi)$ induces parametric processes between the modes. The choice of the pump frequency ω_p determines which processes are resonant; i.e., driving at the sum of the oscillators' frequencies leads to amplification, while driving at the frequency difference induces frequency conversion.

In the active-lattice setup one unit cell consists of three oscillators which are nondegenerate in frequency. The oscillators are pairwise connected via the tunable couplers realizing the lattice Hamiltonian in Eq. (1) if all oscillator pairs are

driven at the respective frequency difference of each pair. In principle, this would require three different pump frequencies ω_p per unit cell. However, it is possible to reduce the number of pump sources by using second harmonics of the pumps [31] and by designing a dual-frequency node-oscillator lattice with link oscillators which are degenerate in frequency; see Fig. 7(a).

A second implementation is based on the Josephson parametric converter (JPC) [33]; see Fig. 7(b). The JPC realizes three-wave mixing and can be operated as a reciprocal or nonreciprocal quantum limited amplifier [16]. The coupling elements of the JPC are based on the Josephson ring modulator (JRM), a ring which consists of four Josephson junctions arranged in a Wheatstone bridge configuration. Each JRM supports three orthogonal electric modes (X, Y, Z) and by treating the ring by a flux Φ close to half a flux quantum this device realizes three-wave mixing between these modes [33]. Combining the JRM with microstrip resonators realizes the JPC, a purely dispersive device which realizes the quadratic interactions necessary for the active-lattice setup.

The coupling between linear resonators could as well be realized via a superconducting interference device (SQUID). A SQUID-based tunable three-oscillator element has recently been used to implement a nonreciprocal frequency converter that can *in situ* be reconfigured to a phase-preserving directional amplifier [18]. A further design option involves the replacement of the link oscillator by a strongly damped qubit or a mechanical resonator. The latter could be phononic modes of an optomechanical crystal [17] or an electromechanical drumhead resonator [19,20]. Further details for the case of a JPC and a qubit implementation are found in the Appendices.

We would like to note that based on parametric modulations in an oscillator lattice (without dissipation), one could in

principle construct topologically nontrivial band structures exhibiting one-way edge modes. However, the latter requires a high amount of control over the whole lattice. Moreover, a certain lattice size is necessary to allow for a clear separation of edge states from the bulk, i.e., to prevent scattering from the edge into the bulk states. In contrast, our proposed scheme works for arbitrary lattice size and in principle only the phases and couplings of the signal-carrying oscillators and their nearest neighbors have to be fixed. The remaining oscillators do not affect the transmission properties of the lattice and hence, the amount of control is much less than in a topologically based scheme.

VIII. CONCLUSION

Optimal routing of signals in a large-scale quantum information processor comes with certain requirements: on-chip implementation of as many components as possible, quantum limitedness, robustness to imperfections, and protection of signal sources from unwanted back reflections. We introduced a 2D superconducting circuit architecture which allows the nonreciprocal routing of excitations at the quantum level, and which can achieve all the desired characteristics. We showed that by engineering the interactions in a dual-lattice design we obtain full control over the propagation path of a signal injected into the structure.

Nonreciprocal routing in a lattice via dissipation engineering exhibits notable new features with respect to topological approaches: (1) there exist no apparent topological quantum numbers associated with lattices composed of parametrically driven units; (2) the transport is controlled by a non-Hermitian matrix, which is parametrically dependent on drive amplitudes and frequencies; (3) the appearance of exceptional points, which are special degeneracies of a non-Hermitian matrix; and (4) the lattices can be designed to amplify input signals near the standard quantum limit.

The implementation of the proposed active lattice requires a layout that will allow the full control over the modulated elements, while keeping their cross-talk to a minimum. This is a formidable challenge that all quantum information processing schemes have to face. A promising route in this direction is a multilayer architecture which would place the lattice on one chip and the control lines for modulation in another layer. Efforts in this direction are underway in several laboratories [14,34,35].

ACKNOWLEDGMENTS

APPENDIX A: ONE-WAY TRANSPORT BETWEEN TWO CONNECTED NODES

We first discuss the basic ingredients of the proposed active lattice, namely the implementation of one-way transport between two given nodes $i \rightarrow j$. We start out from the effective lattice Hamiltonian given in Eq. (1) of the main text and derive the Heisenberg-Langevin equations of motion for two sites i and j and the link oscillator ij:

$$\dot{\hat{d}}_i = -iG_{ij}e^{-i\phi_{ij}}\hat{d}_j - iG_{i;ij}\hat{d}_{ij},$$

$$\dot{\hat{d}}_j = -iG_{ij}e^{i\phi_{ij}}\hat{d}_i - iG_{j;ij}\hat{d}_{ij}, \tag{A1}$$

$$\dot{\hat{d}}_{ij} = -\frac{\kappa_{ij}}{2}\hat{d}_{ij} - \sqrt{\kappa_{ij}}\hat{d}_{ij,\text{in}} - iG_{i;ij}\hat{d}_i - iG_{j;ij}\hat{d}_j.$$

Here we assumed that the link oscillator is coupled to an equilibrium bath with rate κ_{ij}, and that κ_{ij} is the dominant loss channel in the system, comparable to G_{ij}; $\hat{d}_{ij,\text{in}}$ describes thermal and vacuum noise driving the link oscillator. As discussed below, the satisfaction of this condition is no requirement for directionality, but will suppress the reverse propagating signal for a broader range of frequencies. Adiabatically eliminating $\hat{d}_{ij}$, we obtain the Heisenberg-Langevin equations of motion for the two sites i and j:

$$\dot{\hat{d}}_i = -\frac{\Gamma_{i;ij}}{2}\hat{d}_i + i\sqrt{\Gamma_{i;ij}}\hat{d}_{ij,\text{in}}$$

$$- \left[iG_{ij}e^{-i\phi_{ij}} + \frac{\sqrt{\Gamma_{i;ij}\Gamma_{j;ij}}}{2} \right]\hat{d}_j,$$

$$\dot{\hat{d}}_j = -\frac{\Gamma_{j;ij}}{2}\hat{d}_i + i\sqrt{\Gamma_{j;ij}}\hat{d}_{ij,\text{in}}$$

$$- \left[iG_{ij}e^{+i\phi_{ij}} + \frac{\sqrt{\Gamma_{i;ij}\Gamma_{j;ij}}}{2} \right]\hat{d}_i, \tag{A2}$$

with the definitions $\Gamma_{n;ij} = 4G_{n;ij}^2/\kappa_{ij}, (n \in i,j)$. In this damped link oscillator regime the system of two node oscillators can as well be described via a Markovian master equation, where the dissipative interaction is described via the nonlocal superoperator

$$\Gamma_{i;ij}\mathcal{L}\left[\hat{d}_i + \sqrt{\frac{\Gamma_{j;ij}}{\Gamma_{i;ij}}}\hat{d}_j \right]\hat{\rho}, \tag{A3}$$

with $\mathcal{L}[\hat{o}]\hat{\rho} = \hat{o}\hat{\rho}\hat{o}^\dagger - \frac{1}{2}\hat{o}^\dagger\hat{o}\hat{\rho} - \frac{1}{2}\hat{\rho}\hat{o}^\dagger\hat{o}$. Thus, the link oscillator can be interpreted as an engineered reservoir for the node oscillators, which has two important effects. It gives rise to an indirect exchange term between two node oscillators, while inducing local damping at a rate $\Gamma_{n;ij}/2$.

We aim for the situation where the oscillator j is driven by the oscillator i but not vice versa. This can be achieved through balancing the effective dissipative hopping term, i.e., the second term in the square brackets in Eq. (A2), with the unitary hopping term [12]. The balancing conditions become

$$\phi_{ij} \equiv -\frac{\pi}{2} \quad \text{and} \quad G_{ij} \equiv \frac{\sqrt{\Gamma_{i;ij}\Gamma_{j;ij}}}{2}. \tag{A4}$$

These conditions provide a manifestly directional coupling for excitations (j is coupled to i but not vice versa):

$$\dot{\hat{d}}_i = -\frac{\Gamma_{i;ij}}{2}\hat{d}_i + \sqrt{\Gamma_{i;ij}}\hat{d}_{ij,\text{in}},$$

$$\dot{\hat{d}}_j = -\frac{\Gamma_{j;ij}}{2}\hat{d}_i + \sqrt{\Gamma_{j;ij}}\hat{d}_{ij,\text{in}} - \sqrt{\Gamma_{i;ij}\Gamma_{j;ij}}\hat{d}_i. \tag{A5}$$

This mechanism should be contrasted to earlier work in lattices subject to artificial gauge fields [14], where dissipation is desired to be minimal. In the latter case, directional propagation is a pure interference effect and can be described through Hamiltonian dynamics, and therefore it is more appropriate to talk about the breaking of time-reversal symmetry.

APPENDIX B: NONRECIPROCAL PROPAGATION ALONG A 1D CHAIN

In this section we provide further details for the example of nonreciprocal transport along a chain of oscillators. The oscillator chain consists of N oscillators with alternating resonant frequencies $\omega_{1,2}$. Each oscillator pair is coupled via a coherent hopping interaction and we assume equal couplings $G_{ij}e^{-i\phi_{ij}} \equiv J$ between oscillator i and $j = i + 1$. For better overview, we as well assume a uniform coupling to the link oscillators, i.e., we set $G_{i;ij} \equiv \lambda$, and we denote the link oscillators here as $\hat{d}_{ii+1} \equiv \hat{c}_i$. Moving to a frame with respect to each oscillator's resonant frequency the final Hamiltonian reads

$$\hat{\mathcal{H}} = \sum_{i=1}^{N} \delta_i \hat{d}_i^\dagger \hat{d}_i + \sum_{i=1}^{N-1} [J \hat{d}_i^\dagger \hat{d}_{i+1} + \lambda \hat{c}_i^\dagger (\hat{d}_i + \hat{d}_{i+1}) + \text{H.c.}].$$

(B1)

Here we take into account the detunings $\delta_i = \omega_i - \omega_{1,2}$. These detunings can be a consequence of the oscillators' resonant frequencies deviating from $\omega_{1,2}$ or from those of the external driving frequencies that are necessary to obtain the interactions in Eq. (B1) as further discussed in Appendix D.

We assumed that oscillators 1 and N are coupled to external waveguides with coupling strength κ_e; additionally, all oscillators are coupled to Markovian baths with coupling strength η. The latter is introduced to evaluate the impact of finite loss acting on the node oscillators. We adiabatically eliminate the link oscillators and apply the directionality condition $J = i\frac{\Gamma}{2}$ with $\Gamma = 4\lambda^2/\kappa_{ij}$. By impedance-matching the system via $\Gamma = \kappa$ we obtain the equation system

$$\frac{d}{dt}\hat{d}_1 = -\sqrt{\kappa_e}\hat{d}_{1,\text{in}} - \sqrt{\eta}\hat{\xi}_{1,\text{in}} + i\sqrt{\kappa}\hat{c}_{1,\text{in}} - (i\delta_1 + \kappa)\hat{d}_1,$$

$$\frac{d}{dt}\hat{d}_m = -\sqrt{\eta}\hat{\xi}_{m,\text{in}} + i\sqrt{\kappa}\hat{c}_{m-1,\text{in}} + i\sqrt{\kappa}\hat{c}_{m,\text{in}}$$
$$- \left(i\delta_m + \frac{\eta + 2\kappa}{2}\right)\hat{d}_m - \kappa\hat{d}_{m-1}, \quad m \in [2, N-1],$$

$$\frac{d}{dt}\hat{d}_N = -\sqrt{\kappa_e}\hat{d}_{N,\text{in}} - \sqrt{\eta}\hat{\xi}_{N,\text{in}} + i\sqrt{\kappa}\hat{c}_{N-1,\text{in}}$$
$$- (i\delta_N + \kappa)\hat{d}_N - \kappa\hat{d}_{N-1}$$

(B2)

with $\kappa = \kappa_e + \eta$. $\hat{\xi}_{i,\text{in}}$ describe thermal and vacuum fluctuation impinging on each oscillator, while $\hat{c}_{m,\text{in}}$ correspond to the noise contribution arising due to the coupling to the link oscillators. Although we obtain a system of N coupled equations, it is possible to obtain analytic expressions for the scattering parameters. Using input-output theory, $\hat{d}_{i,\text{out}} = \hat{d}_{i,\text{in}} + \sqrt{\kappa_e}\hat{d}_i$,

we can derive the transmission coefficient

$$\mathcal{T}[0] = \frac{\left(1 - \frac{\eta}{\kappa}\right)^2}{\left[1 + \frac{\delta_1^2}{\kappa^2}\right]\left[1 + \frac{\delta_N^2}{\kappa^2}\right]} \prod_{m=2}^{N-1} \frac{1}{\left[1 + \frac{\eta}{2\kappa}\right]^2 + \frac{\delta_m^2}{\kappa^2}}$$

$$\stackrel{\delta_i \equiv \delta}{=} \left[\frac{1 - \frac{\eta}{\kappa}}{1 + \frac{\delta^2}{\kappa^2}}\right]^2 \left[\left(1 + \frac{\eta}{2\kappa}\right)^2 + \frac{\delta^2}{\kappa^2}\right]^{2-N}$$

$$\simeq 1 - N\left(\frac{\eta}{\kappa} + \frac{\delta^2}{\kappa^2}\right),$$

(B3)

with $\hat{d}_{N,\text{out}} = t[0]\hat{d}_{1,\text{out}}$ and $\mathcal{T}[0] \equiv |t[0]|^2$. To reach close to unity transmission, the detunings δ/κ and the intrinsic losses η/κ have to be kept at minimum. The length of the oscillator chain becomes important, as with the number of oscillators exposed to decay channels the number of loss channels increases. On the other hand, having finite detunings and intrinsic losses does not impact the nonreciprocity of the system. This can be seen by considering the output of the first oscillator

$$\hat{d}_{1,\text{out}} = \frac{\frac{\eta}{\kappa} + i\frac{\delta_1}{\kappa}}{1 + i\frac{\delta_1}{\kappa}}\hat{d}_{1,\text{in}} - \frac{\sqrt{1 - \frac{\eta}{\kappa}}}{1 + i\frac{\delta_1}{\kappa}}\left[\sqrt{\frac{\eta}{\kappa}}\hat{\xi}_{1,\text{in}} - i\hat{c}_{1,\text{in}}\right];$$

(B4)

crucially, the output does not contain any contributions from oscillators higher up in the chain. The first term simply denotes the reflection of an input signal $\hat{d}_{1,\text{in}}$, while the second term describes the noise contribution from the first link oscillator and the bath of oscillator 1. However, one still aims for a small output of oscillator 1 to protect the source providing the input signal, if that is desired. For the optimal case of $\eta/\kappa, \delta_1/\kappa \to 0$ the output simply becomes $\hat{d}_{1,\text{out}} = i\hat{c}_{1,\text{in}}$; i.e., even in a perfect setting we have an effective noise temperature at the output oscillator 1 which is determined by the first engineered reservoir. Hence, a cold bath driving the link oscillator is desirable.

A further crucial aspect is the noise which is added to the signal while passing down the oscillator chain. The total output of the oscillator N is given by

$$\hat{d}_{N,\text{out}} = \frac{\eta}{\kappa}\hat{d}_{N,\text{in}} - \frac{\sqrt{\kappa_e \eta}}{\kappa}\left[\hat{\xi}_{N,\text{in}} + \frac{(-1)^{N-1}}{\left[1 + \frac{\eta}{2\kappa}\right]^{N-2}}\hat{\xi}_{1,\text{in}}\right]$$

$$- \frac{\sqrt{\kappa_e \eta}}{\kappa} \sum_{k=2}^{N-1} \frac{(-1)^{N-k}}{\left[1 + \frac{\eta}{2\kappa}\right]^{N-k}}\left[\hat{\xi}_{k,\text{in}} + \frac{i}{2}\sqrt{\frac{\eta}{\kappa}}\hat{c}_{k,\text{in}}\right]$$

$$+ t[0]\hat{d}_{1,\text{in}}.$$

(B5)

Here we considered the limit $\delta_i/\kappa \to 0$ as the expression including finite detunings is rather cumbersome. The output contains contributions from all oscillators, except for the first link oscillator as this contribution ends up in the output of oscillator 1, as discussed above. To characterize the noise properties we calculate the symmetric noise spectral density, defined as

$$\bar{S}_{N,\text{out}}[\omega] = \frac{1}{2}\int \frac{d\Omega}{2\pi}\langle\{\hat{d}_{N,\text{out}}[\omega], \hat{d}_{N,\text{out}}^\dagger[\Omega]\}\rangle;$$

(B6)
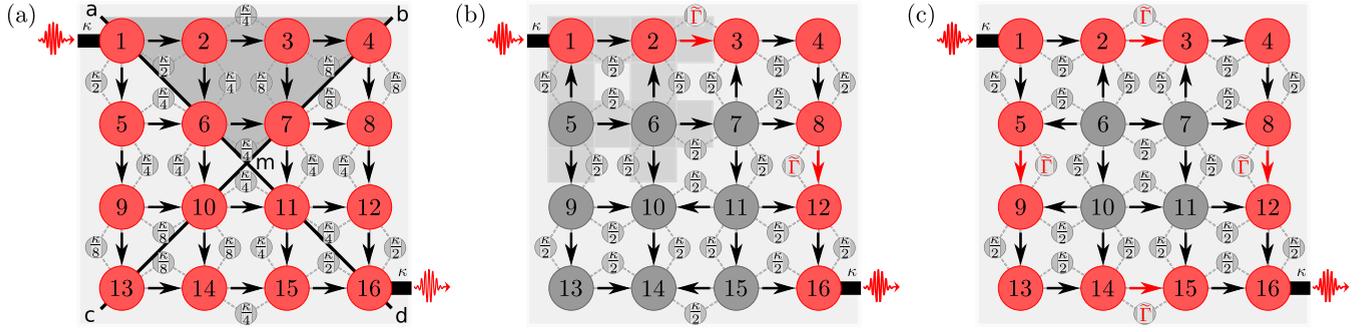
FIG. 8. Example of a 16-oscillator lattice with a staggered coupling pattern (a) or uniform coupling strengths [(b), (c)]. Three different ways to propagate through the structure are highlighted in red. The black arrows indicate which direction is chosen via matching the phase ϕ_{ij} and the effective strength of the interactions $\Gamma_{i,j}$. The respective values for the latter are denoted in the graph, where $\Gamma_{i,j} = \widetilde{\Gamma}$ corresponds to an amplification stage between two oscillators. For the case of propagating over all node oscillators, i.e., graph (a), the staggered coupling pattern exploits the symmetry of the lattice. Here the coupling pattern in the triangle formed between the points **(a m b)** (gray-shaded area) can be mirrored along both diagonals to give the coupling pattern in the triangles **(b m d)** and **(a m c)**, mirroring the latter once more along the diagonal **(c b)** results in the couplings in the remaining triangle **(c m d)**.

for the evaluation we use the noise correlators $\langle \hat{o}_{\text{in}}[\omega]\hat{o}_{\text{in}}^\dagger[\Omega]\rangle = \langle \hat{o}_{\text{in}}^\dagger[\omega]\hat{o}_{\text{in}}[\Omega]\rangle + 2\pi\delta(\omega+\Omega) = 2\pi\delta(\omega+\Omega)(\bar{n}_o^T+1)$, where $o = \xi_i, c_k, d_{1,N}$. The output noise spectral density on resonance yields

$$\bar{S}_{N,\text{out}}[0] = \frac{1}{2} + \frac{\left[1-\frac{\eta}{\kappa}\right]}{\left[1+\frac{\eta}{2\kappa}\right]^{2(N-2)}}\left\{\left[1-\frac{\eta}{\kappa}\right]\bar{n}_{d_1}^T + \frac{\eta}{\kappa}\bar{n}_{\xi_1}^T\right\}$$
$$+ \frac{\eta}{\kappa}\left[\frac{\eta}{\kappa}\bar{n}_{d_N}^T + \left[1-\frac{\eta}{\kappa}\right]\bar{n}_{\xi_N}^T\right]$$
$$+ \sum_{k=2}^{N-1}\frac{\frac{\eta}{\kappa}\left[1-\frac{\eta}{\kappa}\right]}{\left[1+\frac{\eta}{2\kappa}\right]^{2(N-k)}}\left[\bar{n}_{\xi_k}^T + \frac{\eta}{4\kappa}\bar{n}_{c_k}^T\right]. \quad \text{(B7)}$$

Here the second term describes the thermal noise originating from oscillator 1, while the terms in the square brackets denote noise contributions from the remaining node oscillators and link oscillators. For the case of negligible intrinsic losses, the contribution which is always present is noise associated with the input signal, i.e., $\bar{S}_{N,\text{out}}[0] \rightarrow 1/2 + \bar{n}_{d_1}^T$ for $\eta/\kappa \rightarrow 0$. However, if one assumes thermal baths $\bar{n}^T$ with equal temperatures for all oscillators, the output spectrum is independent of the ratio η/κ, $\bar{S}_{N,\text{out}}[0] = (\bar{n}^T+\frac{1}{2})$. Crucially, the thermal noise contribution of the link oscillators scales quadratically with η/κ. This becomes clearer if we set $\bar{n}_{d_{1,N},\xi_i}^T \equiv \bar{n}_d^T$ and $\bar{n}_{c_k}^T \equiv \bar{n}_{\text{link}}^T$ and expand the output noise for small values of η/κ:

$$\bar{S}_{N,\text{out}}[0] = \frac{1}{2} + \bar{n}_d^T + \frac{1}{2}\left[\frac{N}{2}-1\right](\bar{n}_{\text{link}}^T-\bar{n}_d^T)\frac{\eta^2}{\kappa^2} + O\left[\frac{\eta^3}{\kappa^3}\right].$$
$$\text{(B8)}$$

The reason for this quadratic scaling lies in an interference effect; neighboring node oscillators are coupled to the same link oscillator and hence, part of the noise originating from the link oscillator cancels out.

APPENDIX C: NONRECIPROCAL PROPAGATION IN 2D

Now we turn to the details of nonreciprocal signal propagation in two dimensions. By tuning the coupling strengths and

the phases in our setup we can choose an arbitrary path through a 2D lattice of N^2 oscillators. We focus on three different paths: propagation over all oscillators, along one edge, and along both edges; see Fig. 8 for the example of a 16-oscillator lattice. The arrows between each oscillator denote the direction of the signal/information transfer, which is determined via the phase ϕ_{ij}. Depending on the chosen direction the latter takes the following values:

$$\downarrow, \rightarrow: \phi_{ij} = -\frac{\pi}{2}, \quad \uparrow, \leftarrow: \phi_{ij} = +\frac{\pi}{2}. \quad \text{(C1)}$$

We assume that each oscillator pair couples with the same strength to their respective link oscillator; i.e., we set $\Gamma_{n,ij} \equiv \Gamma_{i,j}$. Hence, the remaining directionality condition between two oscillators simplifies to $G_{ij} = \Gamma_{i,j}/2$. After applying the latter condition we end up with an effective unidirectional coupling of oscillator i and j with strength $\Gamma_{i,j}$; cf. Eq. (A5). The optimal values for these effective couplings $\Gamma_{i,j}$ are chosen depending on the respective propagation path through the lattice as illustrated in the following sections.

1. Hopping over all oscillators

We start with the illustration of the special case of hopping over all oscillator nodes. Here the signal passes through all oscillators, and all phases are set to $\phi_{ij} = -\frac{\pi}{2}$; i.e., the signal propagates to the right and downwards. Although propagation over all oscillators is not a distinct propagation path, it comprised a couple of interesting properties worth pointing out. As mentioned in the main text, the point of directionality here marks a transition from oscillatory to purely damped dynamics (in an appropriately rotated frame). Moreover, it allows for unity transmission without involving an amplification stage; i.e., it is possible to match the sum of the local damping experienced by each mode to the coupling to its neighbors from which it receives the input signal. This means that a signal has to be passed on faster than it can leak out of an oscillator.

To realize unity transmission through the lattice we have to create a pattern of staggered coupling strengths. To derive this pattern we can exploit the symmetry of the lattice. For simplicity, we focus on an N^2 lattice with N being even, but a

generalization is straightforward. We divide the square lattice along its diagonals into four equal triangles; for an example see Fig. 8(a). Now we only have to define the couplings in one of these triangles and can then obtain all remaining couplings via mirroring the coupling pattern along the diagonals. Overall, we follow the simple rule that along the upper edge the effective coupling between two neighbors m and $m+1$ decreases as $\kappa/2^m$, reaching $\kappa/2^{N-1}$ at the corner. The same holds for the left edge and is reversed for the lower and right edge, while the inner couplings have to be adjusted accordingly. For example taking the triangle involving the upper edge, e.g., the gray-shaded area in Fig. 8(a) for $N = 4$, the staggered couplings for arbitrary lattice size are set via

$$\Gamma_{m,m+1} = \frac{\kappa}{2^m}, \quad m = 1, \ldots, N-1;$$

$$\Gamma_{nN+m,nN+m+1} = \frac{\kappa}{2^m}, \quad n = 1, \ldots, \frac{N}{2} - 1,$$
$$m = 2, \ldots, N - 2n;$$

$$\Gamma_{n(N+1)+m,n(N+1)+m+N} = \frac{\kappa}{2^m}, \quad n = 0, \ldots, \frac{N}{2},$$
$$m = 2, \ldots, N - (2n-1). \tag{C2}$$

This corresponds to a decrease in the coupling strengths from the left side of the triangle to the right side. The couplings scale with $\kappa/2^m$ which follows from the fact that each node oscillator in this triangle effectively acts as a beam splitter; i.e., the signal is fed into oscillator 1 with strength κ and then passed on to oscillator 2 with strength $\kappa/2$ and so on. The remaining couplings in the lattice can then be obtained via mirroring the pattern of the triangle along the diagonals; see Fig. 8(a) for the example of a 16-oscillator lattice.

To illustrate the reason behind the chosen pattern of coupling strengths a bit further, we consider the example of a 16-oscillator lattice; cf. Fig. 8(a). Assuming that all directionality conditions are matched, the expectation values of the signal oscillator 1 and its right neighbor oscillator 2 evolve as

$$\frac{d}{dt}\bar{d}_1 = -\frac{\kappa + \Gamma_{1,2} + \Gamma_{1,5}}{2}\bar{d}_1 - \sqrt{\kappa}d_{1,\text{in}},$$

$$\frac{d}{dt}\bar{d}_2 = -\frac{\Gamma_{1,2} + \Gamma_{2,3} + \Gamma_{2,6}}{2}\bar{d}_2 - \Gamma_{1,2}\bar{d}_1. \tag{C3}$$

Here the coupling to the external waveguide of oscillator 1 is associated with local damping in the amount of $\kappa/2$. Additionally, the dissipative couplings to oscillators 2 and 5 result in local dampings $\Gamma_{1,2;1,5}/2$, respectively. For impedance matching we need $\Gamma_{1,2} + \Gamma_{1,5} \equiv \kappa$ to kill the reflection of the input signal. A symmetric choice is simply $\Gamma_{1,2} = \Gamma_{1,5} = \kappa/2$. On the other hand, oscillator 2's local damping equals $(\Gamma_{1,2} + \Gamma_{2,3} + \Gamma_{2,6})/2$, while its coupling to oscillator 1 is $\Gamma_{1,2} = \kappa/2$. To transfer the input signal fast enough we need $\Gamma_{2,3} + \Gamma_{2,6} = \kappa/2$, leading to the stationary solution $\bar{d}_2 = -\bar{d}_1$, which is exactly what we were after. Crucially, the effective coupling rate between two oscillators has decreased; i.e., for symmetric choice we have $\Gamma_{2,3} = \Gamma_{2,6} = \kappa/4$. Overall, matching the local damping and the effective coupling between all oscillators for the whole 16-oscillator setup leaves us with a pattern of staggered coupling strengths as illustrated in Fig. 8(a) and

given by Eq. (C2). This results in perfect transmission of the input signal; i.e., we have $\bar{d}_{16,\text{out}} = -d_{1,\text{in}}$ as desired. The latter hold true for arbitrary lattice sizes.

The discussed pattern for the coupling strengths results in unity transmission, as denoted above. However, under realistic conditions each oscillator would experience losses due to the coupling to its environment. To study the influence of intrinsic losses, we consider again the example of a 16-oscillator lattice, where we couple each oscillator to a Markovian bath with rate η. The transmission becomes

$$\mathcal{T}_{\text{hopp}}[0] = \left(\frac{\kappa - \eta}{4\eta + 3\kappa}\frac{\kappa^4}{[\eta + \kappa]^4}\right)^2\left[1 + \frac{\eta + \kappa}{2\eta + \kappa}\right.$$
$$\left. + \frac{1}{4}\frac{[\eta + \kappa]^2}{[2\eta + \kappa]^2}\left(1 + \frac{4\eta + 3\kappa}{4\eta + \kappa}\right)\right]^2$$
$$= 1 - 16\frac{\eta}{\kappa} + \frac{428}{3}\frac{\eta^2}{\kappa^2} + O\left[\frac{\eta^3}{\kappa^3}\right]. \tag{C4}$$

In the second step we expanded the result for small ratios η/κ. In the limit $\eta/\kappa \to 0$ we have unity transmission. The expanded expression of the transmission for finite losses makes clear what happens when the signal passes through the lattice: we have 16 intermediate oscillators; thus in every one of these oscillators we lose approximately an η/κ part of the signal. The corresponding added noise follows the same logic:

$$\bar{n}_{\text{add}} = 16\left(\bar{n}_d^T + \frac{1}{2}\right)\frac{\eta}{\kappa}$$
$$+ \left\{\frac{293}{3}\left[\bar{n}_d^T + \frac{1}{2}\right] + \frac{563}{36}\left[\bar{n}_{\text{link}}^T + \frac{1}{2}\right]\right\}\frac{\eta^2}{\kappa^2} + O\left[\frac{\eta^3}{\kappa^3}\right], \tag{C5}$$

where we assumed equal thermal baths $\bar{n}_{\text{link}}^T$ for all link oscillators, as well as for all node oscillators ($\bar{n}_d^T$). Every node oscillator contributes at least their vacuum fluctuations to the added noise. The contribution from the fluctuations of the link oscillators is less damaging as it scales with $(\eta/\kappa)^2$. However, for $\eta/\kappa = 0$ we have no added noise corresponding to the optimal situation.

While the intrinsic losses do influence the transmission, they do not affect the directionality of the system. This can easily be seen; if we calculate the spectral output noise density for oscillator 1, on resonance we obtain

$$\bar{S}_{1,\text{out}}[0] = \frac{1}{2} + \bar{n}_{\text{link}}^T + \frac{\eta}{\kappa}\left(\bar{n}_{\xi_1}^T - \bar{n}_{\text{link}}^T\right) + \frac{\eta^2}{\kappa^2}\left(\bar{n}_{d_1}^T - \bar{n}_{\xi_1}^T\right), \tag{C6}$$

where $\bar{n}_{\xi_1}^T$ denotes the averaged thermal occupation of the intrinsic oscillator-1 bath and $\bar{n}_{d_1}^T$ is associated with the thermal fluctuations accompanying a possible input signal. The output noise of oscillator 1 contains contributions from the link oscillators which couple it to oscillators 2 and 5. Crucially, besides the two reservoirs and the fluctuations impinging on oscillator 1, there is no further contribution from other node oscillators; i.e., oscillator 1 is perfectly decoupled from the lattice.

2. Propagation along one edge

Next we consider propagation along one edge of the lattice. Here we can avoid a staggered coupling pattern, but as discussed in the main text, for optimal noise performance we have to carefully choose the effective coupling strengths involving the four oscillators in the upper left corner of the lattice, i.e., oscillators $1, 2, N+1$, and $N+2$. We set all remaining effective couplings to $\kappa/2$, except at the amplification stages which we plant between every second oscillator pair along the edge. For the latter case we choose $\Gamma_{i,j} = \widetilde{\Gamma}$ for the effective couplings. Additionally, we have to set the phases ϕ_{ij} in the right manner to ensure propagation only along the edge. Consider for example the signal input oscillator, i.e., oscillator 1; we want to transmit the whole signal to oscillator 2, thus we choose the phase ϕ_{12} in the way that oscillator 1 is decoupled from oscillator 2, while oscillator 2 is driven by oscillator 1; i.e., we set $\phi_{12} = -\pi/2$. To avoid that any information from oscillator 1 is transmitted to oscillator $N+1$ we have to decouple oscillator $N+1$ from oscillator 1 and thus set $\phi_{1,N+1} = +\pi/2$; i.e., the signal cannot enter oscillator $N+1$. We apply this logic along the whole edge of the lattice.

Crucially, one has to fix all couplings between oscillators surrounding the propagation path. However, the remaining couplings and phases are less crucial; e.g., in the 16-oscillator lattice depicted in Fig. 8(b) the lower left block of 4 oscillators (9, 10, 13, 14) can be completely decoupled and the couplings between these oscillators can in principle be set arbitrarily.

With the described coupling pattern the effective coupling of oscillator N^2 to oscillator 1 is of the form

$$\hat{d}_{N^2} = -\frac{1}{2} \prod_{m=2}^{N-1} \sqrt{\mathcal{G}_m}\, \hat{d}_1, \tag{C7}$$

where $\sqrt{\mathcal{G}_m}$ denotes the amplitude gain factors obtained at each oscillator which is coupled to an amplification stage. Importantly, each amplification stage is placed between two oscillators m and $m+1$; hence the product $\sqrt{\mathcal{G}_m \mathcal{G}_{m+1}}$ corresponds to the amplitude gain factor obtained at the whole stage. For the stages with uniform couplings, i.e., $\Gamma_{i,j} = \kappa/2$ for hopping and $\Gamma_{i,j} = \widetilde{\Gamma}$ for amplification, the amplitude gain factors read

$$\sqrt{\mathcal{G}_m} = \frac{\kappa}{\kappa - \widetilde{\Gamma}}, \quad \sqrt{\mathcal{G}_{m+1}} = \frac{2\widetilde{\Gamma}}{\kappa - \widetilde{\Gamma}}, \tag{C8}$$

and the overall transmission coefficient becomes

$$\mathcal{T}_{1\text{edge}}[0] = \frac{\kappa^2}{[\Gamma_{1,2} + \kappa + \Gamma_{1,N+1}]^2} \left[\frac{2\widetilde{\Gamma}\kappa}{(\kappa - \widetilde{\Gamma})^2} \right]^{2(N-3)} \mathcal{G}_2 \mathcal{G}_3, \tag{C9}$$

with the oscillator 2 and 3 amplitude gain factors

$$\sqrt{\mathcal{G}_2} = \frac{2\Gamma_{1,2}}{[\Gamma_{1,2} + \Gamma_{2,N+2} - \widetilde{\Gamma}_{2,3}]},$$

$$\sqrt{\mathcal{G}_3} = \frac{2\widetilde{\Gamma}_{2,3}}{[\Gamma_{3,4} + \Gamma_{3,N+3} - \widetilde{\Gamma}_{2,3}]}, \tag{C10}$$

where we have left the coupling rates involving the four oscillators in the upper left corner of the lattice, i.e., oscillators $1, 2, N+1$, and $N+2$, unspecified. Choosing here as well

uniform couplings ($\Gamma_{i,j} = \kappa/2, \widetilde{\Gamma}$) we recover the forward transmission given in Eq. (7) of the main text.

However, as mentioned above, for optimal noise performance we have to carefully choose the effective coupling strengths in the upper left corner of the lattice. The noise contribution added to the signal before an amplification stage is entered sets the minimum of the added noise. For the case of propagation over one edge the first amplification stage is between oscillators 2 and 3. Thus we have to consider the stationary solution of oscillator 2,

$$\hat{d}_2 = \frac{\sqrt{\mathcal{G}_2}}{\Gamma_{1,2}} \left\{ i\hat{\xi}_2 - \frac{2\Gamma_{1,2}}{\Gamma_{1,2} + \kappa + \Gamma_{1,N+1}} \left[\sqrt{\kappa}\hat{d}_{1,\text{in}} + i\hat{\xi}_1 \right. \right.$$

$$- i\frac{2\Gamma_{1,N+1}}{\Gamma_{1,N+1} + \Gamma_{N+1,N+2} + \Gamma_{N+1,2N+1}}\hat{\xi}_{N+1} \Bigg]$$

$$- i\frac{2\Gamma_{2,N+2}}{\Gamma_{2,N+2} + \Gamma_{N+1,N+2} + \Gamma_{N+2,N+3} + \Gamma_{N+2,2N+2}}$$

$$\left. \left. \times \left[\hat{\xi}_{N+2} - \frac{2\Gamma_{N+1,N+2}}{\Gamma_{1,N+1} + \Gamma_{N+1,N+2} + \Gamma_{N+1,2N+1}}\hat{\xi}_{N+1} \right] \right\} \right. . \tag{C11}$$

The first term in the square brackets is simply the input signal ($\hat{d}_{1,\text{in}}$), while all remaining terms denote the noise contributions $\hat{\xi}_m$ which are added by oscillator m. As illustrated in Fig. 6(a) of the main text, each of these oscillators is exposed to the noise of all link oscillators it couples to; hence, $\hat{\xi}_m$ can be expressed in terms of these contributions:

$$\hat{\xi}_1 = \underline{\sqrt{\Gamma_{1,2}}\hat{d}_{12,\text{in}}} + \sqrt{\Gamma_{1,N+1}}\hat{d}_{1N+1,\text{in}},$$

$$\hat{\xi}_2 = \underline{\sqrt{\Gamma_{1,2}}\hat{d}_{12,\text{in}}} + \underline{\sqrt{\Gamma_{2,N+2}}\hat{d}_{2(N+2),\text{in}}} + \sqrt{\widetilde{\Gamma}_{2,3}}\hat{d}_{23,\text{in}}^\dagger,$$

$$\hat{\xi}_{N+1} = \sqrt{\Gamma_{1,N+1}}\hat{d}_{1(N+1),\text{in}} + \underline{\sqrt{\Gamma_{N+1,N+2}}\hat{d}_{(N+1)(N+2),\text{in}}}$$

$$+ \sqrt{\Gamma_{N+1,2N+1}}\hat{d}_{(N+1)(2N+1),\text{in}},$$

$$\hat{\xi}_{N+2} = \underline{\sqrt{\Gamma_{2,N+2}}\hat{d}_{2(N+2),\text{in}}} + \underline{\sqrt{\Gamma_{N+1,N+2}}\hat{d}_{(N+1)(N+2),\text{in}}}$$

$$+ \sqrt{\Gamma_{N+2,N+3}}\hat{d}_{(N+2)(N+3),\text{in}}$$

$$+ \sqrt{\Gamma_{N+2,2N+2}}\hat{d}_{(N+2)(2N+2),\text{in}}. \tag{C12}$$

Here the underlined contributions can deconstructively interfere at the node oscillator 2, see blue-shaded link oscillators in Fig. 6(a), while the remaining contributions cannot be compensated, i.e., the black-shaded link oscillators in Fig. 6(a). These interferences at the node oscillator 2 are possible because the noise contributions acquire different phase shifts; see Eq. (C11).

The optimal conditions for deconstructive interference at the node oscillator 2 given in Eq. (9) can be extracted from Eq. (C11). As already discussed in the main text, we have to ensure that the noise contributions are transmitted to the node oscillator 2 with unity transmission, i.e., so that all $\hat{\xi}_m$ contributions inside of the wavy brackets in Eq. (C11) come in with the prefactor of $\pm i$. For example, under condition (i), i.e., $\Gamma_{1,2} = \kappa + \Gamma_{1,N+1}$, the noise contribution $\hat{\xi}_1$ originating from oscillator 1 comes in with a prefactor of $-i$ and therewith the same amplitude as $\hat{\xi}_2$, but with a phase shift of π. This phase difference allows for the complete cancellation of the noise
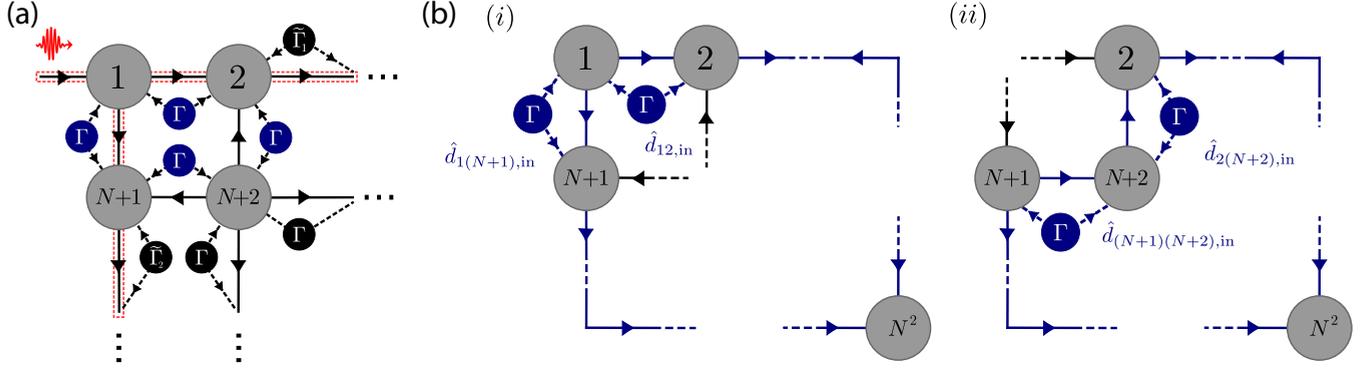
FIG. 9. Noise flow and interference for propagating along both edges. (a) The red dashed area indicates the propagation of the signal injected into the node oscillator 1. Oscillators 2 and $N + 1$ are connected to amplification stages ($\widetilde{\Gamma}_{1,2}$). The noise contributions arising from the blue-shaded link oscillators can deconstructively interfere, while the noise contributions from the black-shaded link oscillators cannot be compensated. (b) Noise path for deconstructive interference at oscillator N^2. Under the optimal conditions in Eq. (C19) the noise contributions from the blue-shaded link oscillators are canceled.

contribution $\hat{d}_{12,\text{in}}$; see Eq. (C12). Similar arguments lead to all three conditions in Eq. (9), and the stationary solution of oscillator 2 becomes ($\mathcal{G}'_2 = \kappa \mathcal{G}_2 / \Gamma^2_{1,2}$)

$$\hat{d}_2 = -\sqrt{\mathcal{G}'_2} \left\{ \hat{d}_{1,\text{in}} + \frac{i}{\sqrt{\kappa}} [\hat{\xi}_1 - \hat{\xi}_2 + \hat{\xi}_{N+2} - \hat{\xi}_{N+1}] \right\},$$

(C13)

where all noise contributions $\hat{\xi}_m$ have now the same prefactor. Inserting their explicit structure given in Eq. (C12), all contributions arriving via a closed loop at oscillator 2 vanish as desired. For zero temperature the symmetrized spectra become

$$\bar{S}_2[0] = \mathcal{G}'_2 \left\{ 1 + (\widetilde{\Gamma}_{\text{opt}} + \Gamma_{1,N+1} + \Gamma_{2,N+2}) \frac{1}{\kappa} \right\} \frac{1}{2}.$$

(C14)

The first term corresponds simply to the noise accompanying an input on oscillator 1, while the remaining noise contributions arise from the coupling to oscillators 3, $N + 1$, and $N + 2$. The gain increases for $\widetilde{\Gamma}_{\text{opt}} \to \kappa + \Gamma_{1,N+1} + \Gamma_{2,N+2}$ and the added noise in the large gain limit can be approximated as

$$\bar{n}_{2,\text{add}} = \frac{\bar{S}_2[0]}{\mathcal{G}'_2} - \frac{1}{2} \to \left\{ \frac{1}{2} + (\Gamma_{1,N+1} + \Gamma_{2,N+2}) \frac{1}{\kappa} \right\},$$

(C15)

which coincides with the added noise for the whole lattice, i.e., $\bar{n}_{\text{add}} \simeq \bar{n}_{2,\text{add}}$. The latter limit is independent of the lattice size as long as the first amplification stage is implemented between oscillators 2 and 3. Note, a simple solution to minimize the added noise here is by setting $\Gamma_{1,N+1} = \Gamma_{2,N+2} = 0$, which effectively reduces the system to a 1D chain.

Finally, we would like to briefly discuss the noise characteristics without optimizing the coupling rates, i.e., by assuming uniform couplings all over the lattice ($\Gamma_{i,j} = \kappa/2, \widetilde{\Gamma}$); here the stationary solution of oscillator 2 reads ($\mathcal{G}'_2 = \mathcal{G}_2/\kappa$)

$$\hat{d}_2 = -\sqrt{\mathcal{G}'_2} \left\{ \hat{d}_{1,\text{in}} - \frac{i}{\sqrt{\kappa}} \left[2\hat{\xi}_2 - \hat{\xi}_1 + \frac{4}{3}\hat{\xi}_{N+1} - \hat{\xi}_{N+2} \right] \right\}.$$

(C16)

For this case, the noise contributions $\hat{\xi}_m$ come in with different prefactors and cannot optimally interfere; the symmetrized noise spectra for oscillator 2 become

$$\bar{S}_2[0] = \mathcal{G}'_2 \left(\bar{n}^T_{d_1} + \frac{1}{2} \right) + \mathcal{G}'_2 \left\{ \frac{4\widetilde{\Gamma}}{\kappa} + 3 \right\} \left(\bar{n}^T_{\text{link}} + \frac{1}{2} \right),$$

(C17)

where we assumed equal bath temperatures for all link oscillators. We can now extract the noise which is added to the input signal at this stage; the added noise referred back to the input yields

$$\bar{n}_{2,\text{add}} = \frac{\bar{S}_2[0]}{\mathcal{G}'_2} - \left(\bar{n}^T_{d_1} + \frac{1}{2} \right) = \left\{ \frac{4\widetilde{\Gamma}}{\kappa} + 3 \right\} \left(\bar{n}^T_{\text{link}} + \frac{1}{2} \right).$$

(C18)

Hence, even in the large-gain limit and for zero temperature, i.e., for $\widetilde{\Gamma} \to \kappa$ and $\bar{n}^T_{\text{link}} = 0$, the added noise is at least 3.5 quanta.

3. Propagation along both edges

As a final example for nonreciprocal signal propagation in a 2D lattice, we consider a path over both edges, where the signal is split at oscillator 1, travels along both edges, and interferes at oscillator N^2. For the example of a 16-oscillator lattice see Fig. 8(c). In a square lattice both pathways are symmetric and simply correspond to a combination of two one-edge cases discussed in the section above; i.e., the signal amplitude is simply doubled at the output oscillator. Hence, the transmission simply gains a factor of 4; i.e., we have $\mathcal{T}_{2\text{edge}}[0] = 4\mathcal{T}_{1\text{edge}}[0]$.

Similarly, the noise added at each path is qualitatively the same and we can optimize the possible deconstructive interference as before. However, in contrast to the one-edge case where the noise flow did interfere at oscillator 2, the noise interferes now at the node oscillator N^2. Hence, we have to consider the noise contributions which propagate along a closed loop to oscillator N^2 as sketched in Fig. 9(b). The first amplification stages are placed between oscillators 2 and 3 on the upper edge and at oscillators $N + 1$ and $2N + 1$ on the left edge; thus we need the stationary solutions of $\hat{d}_2$ and $\hat{d}_{N+1}$, from
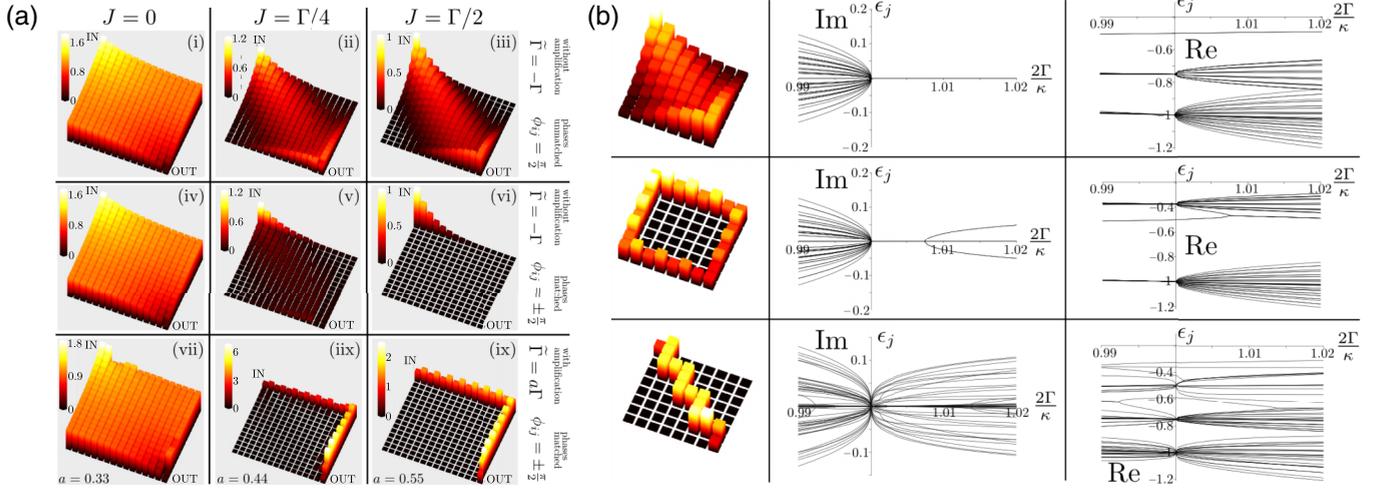
FIG. 10. (a) Averaged steady-state amplitude of each oscillator in a lattice of 256 cavities. The dissipative hopping strength Γ is fixed, while the coherent coupling strength J is increased from the left to right column. Once the directionality conditions are matched, i.e., graphs (vi) and (ix), only the edge cavities have a finite occupation. However, to have a transmission close to unity, amplification stages have to be implemented. (b) Eigenvalues as a function of dissipative coupling strength for an $N = 8$ oscillator lattice for various propagation ways. All eigenvalues are real at the point of directionality $\Gamma = \kappa/2$. The coherent hopping strength is set to $|J| = \kappa/4$ and the dissipative rate Γ is varied. The dynamics at the point of directionality is described by purely real eigenvalues; the latter is independent of the chosen propagation path and the lattice size.

which we can extract two optimal noise canceling conditions:

(i) $\qquad \Gamma_{1,2} + \Gamma_{1,N+1} = \kappa,$

(ii) $\Gamma_{N+1,N+2} + \Gamma_{2,N+2} = \Gamma_{N+2,N+3} + \Gamma_{N+2,2N+2},$ (C19)

where we illustrate in Fig. 9(b) the propagation loops matching both conditions.

At oscillator N^2 both pathways interfere; this means we have to consider the combination of both contributions $\hat{d}_2$ and $\hat{d}_{N+1}$ as they appear in the stationary solution of oscillator $\hat{d}_{N^2}$, i.e., $\hat{d}_{N^2} \sim (\hat{d}_2 + \hat{d}_{N+1})/2 \equiv \hat{D}_{2,N+1}$. Under the conditions given in Eq. (C19) all noise contributions of the link oscillators connecting the four oscillators in the left upper corner cancel and we obtain

$$\frac{\hat{D}_{2,N+1}}{\sqrt{\mathcal{G}_2'}} = \hat{d}_{1,\text{in}} + \frac{i}{\sqrt{\kappa}}\left[\sqrt{\widetilde{\Gamma}_1}\hat{d}_{23,\text{in}}^\dagger + \sqrt{\widetilde{\Gamma}_2}\hat{d}_{(N+1)(2N+1),\text{in}}^\dagger \right.$$
$$+ \sqrt{\Gamma_{N+2,N+3}}\hat{d}_{(N+2)(N+3),\text{in}}$$
$$\left. + \sqrt{\Gamma_{N+2,2N+2}}\hat{d}_{(N+2)(2N+2),\text{in}}\right], \quad \text{(C20)}$$

where we assumed the same gain factor for both amplification stages, i.e.,

$$\sqrt{\mathcal{G}_2'} \equiv \frac{\sqrt{\kappa}}{\Gamma_{1,2} + \Gamma_{2,N+2} - \widetilde{\Gamma}_1} = \frac{\sqrt{\kappa}}{\Gamma_{1,N+1} + \Gamma_{N+1,N+2} - \widetilde{\Gamma}_2},$$
(C21)

and the gain increases for $\widetilde{\Gamma}_1 \to \Gamma_{12} + \Gamma_{2,N+2}$ and $\widetilde{\Gamma}_2 \to \Gamma_{1,N+1} + \Gamma_{N+1,N+2}$. Hence, the noise effectively added after the first two amplification stages can be expressed as

$$\bar{n}_{2,N+1} = \{\widetilde{\Gamma}_1 + \widetilde{\Gamma}_2 + \Gamma_{N+2,N+3} + \Gamma_{N+2,2N+2}\}\frac{1}{2\kappa}$$
$$\to \frac{1}{2} + \frac{1}{\kappa}(\Gamma_{2,N+2} + \Gamma_{N+1,N+2}), \quad \text{(C22)}$$

where we assumed the large gain limit in the second step. For $\Gamma_{2,N+2}, \Gamma_{N+1,N+2} \ll \kappa$ the added noise drops down to half a quantum—the standard quantum limit (SQL) of a phase-insensitive amplifier. As for the one-edge case, the minimum noise value added to a signal leaving the final output port coincides with $\bar{n}_{2,N+1}$ (for large gain). This minimum added noise is again independent of the lattice size; it is solely determined by the first amplification stages.

4. Various propagation paths

A crucial aspect of our setup is that we can choose an arbitrary path through the lattice. We find that, independently of the chosen propagation path and the lattice size, the dynamics at the point of directionality is described by purely real eigenvalues. Figure 10 depicts the results for a 64-oscillator lattice and three different pathways. The case of propagation over all oscillators, i.e., Fig. 10(a) (i), shows similarities to the cavity chain; here the point of directionality coincides with three exceptional points and marks a transition from oscillatory to purely damped dynamics (in the rotated frame).

APPENDIX D: EXAMPLES OF IMPLEMENTATIONS IN A SUPERCONDUCTING LATTICE ARCHITECTURE

There are multiple ways to implement the proposed setup as sketched in Fig. 6 in the main text. In this section we provide further details for these actual implementations. The basic building block could for example consist of three cavity modes representing the two node oscillators and the link oscillator. The three modes are coupled via one or more nonlinear elements which, under appropriate driving, provides the desired interactions between them. Crucially, we require a coherent exchange interaction between the node oscillators,

while the coupling to the link oscillator realizes an indirect exchange interaction. However, instead of using a cavity mode as the link oscillator one could as well use a highly damped qubit which we discuss in detail in the following section.

1. A highly damped qubit as an engineered reservoir

We focus on a single element made out of two node oscillators with frequencies ω_1 and ω_2, which are described by the operators $\hat{d}_1$ and $\hat{d}_2$. We require a coherent hopping interaction of the form

$$\hat{\mathcal{H}}_{\text{hop}} = M(t)\,\hat{d}_1^\dagger \hat{d}_2 + \text{H.c.}, \tag{D1}$$

where $M(t) = G_{12}\cos(\omega_P t + \phi_P)$ is a time-dependent coupling which is modulated by an external pump. Such an interaction can be realized by coupling the two cavities via a superconducting quantum interference device (SQUID) [36–38]. Driving the respective coupling circuit with an external flux at the frequency difference of the cavity modes, i.e., $\omega_P = \omega_1 - \omega_2$, induces resonant hopping between them.

The Hamiltonian in Eq. (D1) realizes reciprocal information transfer between the two cavity modes. To break this symmetry we combine this coherent interaction with an engineered dissipative interaction; i.e., we construct an engineered reservoir which is connected to the two cavity modes and mediates an effective interaction between them. For this we couple both modes to a qubit with transition frequency ω_q. The qubit itself is an open system; i.e., it is coupled with rate γ to an environment which damps its dynamics. As we will see in what follows, the qubit realizes our engineered reservoir in the high damping case, i.e., when its dynamics is much faster than the one of the cavity modes and can effectively be considered to be a Markovian bath for the cavities. The combined system is described by the Hamiltonian

$$\hat{\mathcal{H}} = \frac{\omega_q}{2}\hat{\sigma}_z + \sum_{n=1,2}[\omega_n \hat{d}_n^\dagger \hat{d}_n + g_n(\hat{d}_n + \hat{d}_n^\dagger)\hat{\sigma}_x]. \tag{D2}$$

The qubit and the cavity modes interact via a standard Rabi interaction, where g_n corresponds to the coupling between the individual modes and the qubit; the latter is described by the Pauli operators $\hat{\sigma}_{x,y,z}$. An external drive at frequency Ω modulates the transition frequency of the qubit,

$$\hat{\mathcal{H}}_{\text{drive}} = \Omega\varepsilon\cos(\Omega t + \phi)\hat{\sigma}_z, \tag{D3}$$

a driving scheme which incorporates first-order sideband transition physics [39–42]. This means that by tuning the drive to a sideband at frequencies $\omega_q \pm \omega_n$ (blue/red) one can realize first-order scattering processes between the qubit and the cavity modes. For example, having a tone on the red sideband results in swapping of excitations between the cavity modes and the qubit, a process which conserves the number of excitations. On the other side, having a tone on the blue sideband realizes a two-mode squeezing interaction which generates entanglement and amplification. A possible realization would be an external flux line in the vicinity of a transmon qubit.

In the next step we introduce an interaction picture with respect to the free Hamiltonian for the cavities and the qubit, as well as to the drive Hamiltonian $\hat{\mathcal{H}}_{\text{drive}}$, described by the

unitary transformation

$$U(t) = e^{-i[\omega_1 \hat{d}_1^\dagger \hat{d}_1 + \omega_2 \hat{d}_2^\dagger \hat{d}_2]t}\,e^{-\frac{i}{2}\omega_q t}\,e^{-i\int_0^t dt'\,\hat{\mathcal{H}}_{\text{drive}}(t')}. \tag{D4}$$

Applying this transformation to our system Hamiltonian, i.e., $\hat{\mathcal{H}}' = U^\dagger \hat{\mathcal{H}} U$, leaves us still with a time-dependent Hamiltonian of the form

$$\hat{\mathcal{H}}' = \sum_{n=1,2}\hat{d}_n[G_n^+(t)\hat{\sigma}_- + G_n^-(t)\hat{\sigma}_+] + \text{H.c.},$$

$$G_n^\pm(t) = g_n\sum_{k=-\infty}^{+\infty}J_k(2\varepsilon)e^{-i[\omega_n \pm \omega_q \pm k\Omega]t}\,e^{\mp ik\phi}, \tag{D5}$$

with the time-modulated coupling coefficients $G_n^\pm(t)$. So far this Hamiltonian is exact and involves Raman up- and down-scattering processes between the cavity resonant frequency and the sidebands at $\omega_n \pm \omega_q$. However, by choosing the frequency of the external pump one can engineer the desired resonant interactions in the coupled system. We choose a special hierarchy of the resonant frequencies involved, setting $\omega_1 - \omega_q = \omega_q - \omega_2 = \Delta$ and drive at $\Omega = \Delta$. Then the couplings G_n^- become only secular for $k = \pm 1$; hence, for large enough Δ we can make a rotating wave approximation (RWA) and approximate the couplings to $G_n^-(t) \simeq \pm g_n J_1(2\varepsilon)\,e^{\pm i\phi} \equiv \pm G_n e^{\pm i\phi}$, where the $+$ $(-)$ sign refers to $n = 1$ (2). Setting $G_1 = G_2 \equiv G$ the effective Hamiltonian becomes

$$\hat{\mathcal{H}}'_{\text{eff}} = G(\hat{d}_1 e^{+i\phi} - \hat{d}_2 e^{-i\phi})\hat{\sigma}_+ + \text{H.c.} \tag{D6}$$

The remaining counter-rotating contributions originating from $G_n^-(t)$ are oscillating with $k'\Delta$ where $k' \neq 0$ and can be neglected. Additionally, the counter-rotating terms related to the parametric coupling $G_n^+(t)$ are off resonant for

$$k_1 \neq \frac{\omega_1 + \omega_q}{\omega_1 - \omega_q}, \quad k_2 \neq \frac{\omega_2 + \omega_q}{\omega_q - \omega_2}, \quad k_{1,2} \in \mathbb{Z}, \tag{D7}$$

which can be achieved by appropriate choice of the resonant frequencies.

Finally, we include the coherent hopping given in Eq. (D1) and have now our final building block, a two-cavity unit where we can tune the interaction direction by adjusting the strength and the phase of the drive tone on the qubit together with tuning the coherent interaction. An advantage of the chosen frequency hierarchy is that the pump frequency for the coherent interaction is at $\omega_P = \omega_1 - \omega_2 = 2\Delta$, which is simply the second harmonic of the drive tone on the qubit. Hence, a single pump source is in principle sufficient.

The qubit is tantamount to a cavity mode as a link oscillator. To see this, we assume that the qubit is coupled to a zero-temperature bath with decay rate γ. In the case of a highly damped qubit it can be adiabatically eliminated and the system is modeled via the Lindblad master equation (setting $\varphi \equiv \pi - 2\phi$)

$$\frac{d}{dt}\hat{\rho} = -i[\hat{\mathcal{H}}_{\text{hop}}, \hat{\rho}] + \Gamma\mathcal{L}[\hat{d}_1 + e^{i\varphi}\hat{d}_2]\hat{\rho}, \quad \Gamma = \frac{4G^2}{\gamma}, \tag{D8}$$

with the superoperator $\mathcal{L}[\hat{o}]\hat{\rho} = \hat{o}\hat{\rho}\hat{o}^\dagger - \frac{1}{2}\hat{o}^\dagger\hat{o}\hat{\rho} - \frac{1}{2}\hat{\rho}\hat{o}^\dagger\hat{o}$. This master equation describes the two kinds of interactions
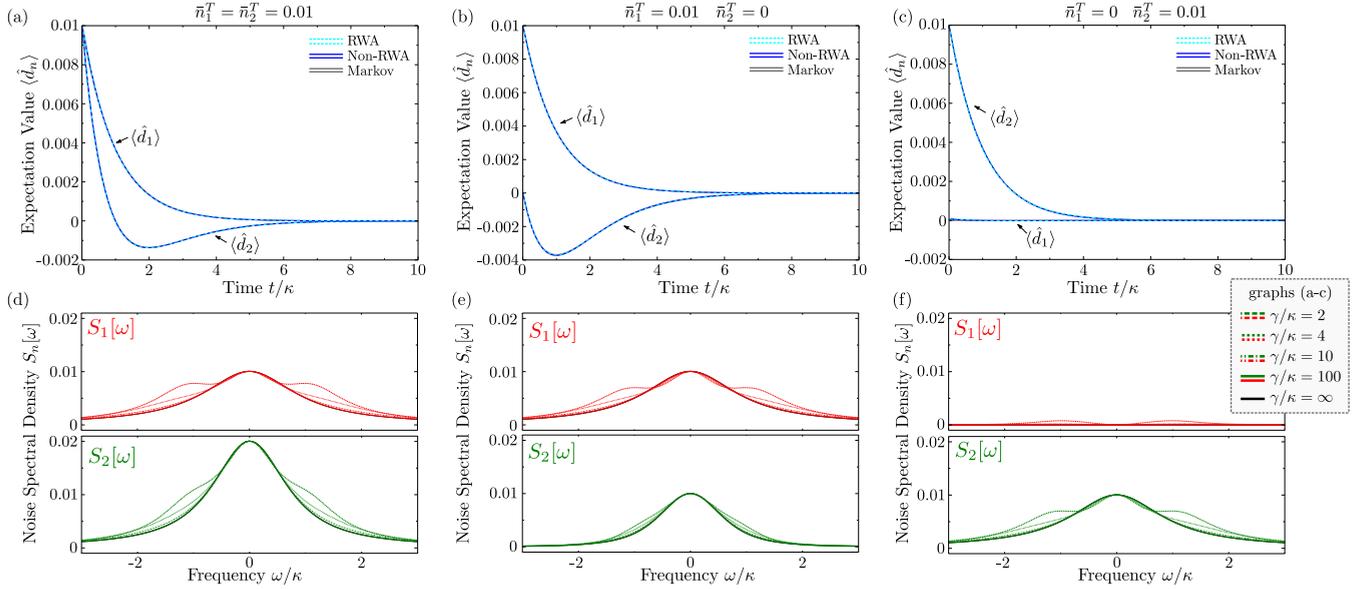
FIG. 11. Numerical simulations of the master equation for the cavities plus qubit system for three different initial conditions. Graphs (a)–(c) depict the dynamics of the cavity expectation values with (RWA) and without (non-RWA) a rotating wave approximation. Here, the non-RWA solution is simulated with the full coherent dynamics of Eq. (D5), while the RWA solutions are simulated with the Hamiltonian given in in Eq. (D6). Additionally, the results for the Markovian limit (Markov) are plotted, i.e., a simulation based on Eq. (D8). Parameters are $\omega_1/\kappa = 1100$, $\omega_2/\kappa = 100$, $\omega_q/\kappa = 600$, and $\gamma/\kappa = 100$. Graphs (d)–(f) depict the noise spectra for both cavities for various values of qubit damping rate γ (as denoted in the graph). For finite rate γ we used a rotating wave approximation, i.e., we simulated Eq. (D6), and compare it to the results for the Markovian master equation (D8). The resulting spectra coincide in the high damping case as expected.

between the cavity modes we were aiming for: the coherent hopping $\hat{\mathcal{H}}_{\text{hop}}$, defined in Eq. (D1), with coupling strength G_{12} and the dissipative hopping with rate Γ assisted by the qubit.

The adiabatic elimination of the qubit is possible in the high damping case; to show that the master equation (D8) describes the system dynamics successfully we perform a numerical simulation of the master equation with the full Hamiltonian using Eqs. (D5) and (D1). We compare our findings to the RWA solution involving Eq. (D6) and the Markovian limit described by Eq. (D8). Figures 11(a)–11(c) depict the resulting dynamics for the cavities' expectation values $\langle d_{1,2} \rangle = \bar{d}_{1,2}$ for three different initial conditions (and assuming always that the directionality conditions are met). In the Markovian limit their time dependence is described via (with $\Gamma = \kappa$)

$$\bar{d}_1(t) = \bar{d}_1(0)e^{-\kappa t}, \qquad \bar{d}_2(t) = \{\bar{d}_2(0) - \bar{d}_1(0)\kappa t\}e^{-\kappa t}. \quad \text{(D9)}$$

The simulated dynamics coincides nicely with these expressions. For the case of finite occupation of each cavity at time $t = 0$, i.e., $\bar{d}_1(0) = \bar{d}_2(0)$, the expectation values decay fast and $\bar{d}_2(t)$ becomes negative at $t/\kappa = 1$ as expected; cf. Fig. 11(a). Crucially, for $\bar{d}_1(0) = 0$ and finite $\bar{d}_2(0)$ the dynamics of cavity 1 is unaffected, while for the reversed initial conditions excitations are transferred from cavity 1 to 2; see Figs. 11(c) and 11(b), respectively.

Figures 11(d)–11(f) depict the resulting noise spectral densities as a function of frequency. Here we compare the RWA solution involving Eq. (D6) for various values of γ and the Markovian limit described by Eq. (D8). In the large damping regime the analytical solutions for the noise spectra

are ($\bar{n}_{\text{link}}^T = 0$)

$$S_1[\omega] = \frac{1}{\kappa} \frac{\bar{n}_{d_1}^T}{\left(1 + \frac{\omega^2}{\kappa^2}\right)},$$

$$S_2[\omega] = \frac{1}{\kappa} \left[\frac{\bar{n}_{d_2}^T}{\left(1 + \frac{\omega^2}{\kappa^2}\right)} + \frac{\bar{n}_{d_1}^T}{\left(1 + \frac{\omega^2}{\kappa^2}\right)^2} \right]. \quad \text{(D10)}$$

Here the cavity-1 spectrum has no contribution from cavity 2. These expressions require a large enough damping γ/κ of the qubit. However, on resonance ($\omega = 0$) the system is always nonreciprocal; see Figs. 11(d)–11(f). Crucially, the damping γ/κ determines the frequency range over which one obtains directionality.

2. Implementation with a Josephson parametric converter

Another possible implementation is based on the Josephson ring modulator [33,43], which is a ring intersecting four Josephson junctions realizing three-wave mixing. Embedding the latter element into a circuit with three microwave resonators enables quantum-limited amplification and conversion of microwave signals; the complete circuit is called a Josephson parametric converter (JPC) [33]. Moreover, the JPC can be operated in a nonreciprocal mode, which was recently demonstrated in Ref. [16]. In the following we recall the basic ideas of this mode of operation. The basic system Hamiltonian of the JPC yields

$$\hat{\mathcal{H}} = \omega_a \hat{a}^\dagger \hat{a} + \omega_b \hat{b}^\dagger \hat{b} + \omega_c \hat{c}^\dagger \hat{c} + g_3(\hat{a} + \hat{a}^\dagger)(\hat{b} + \hat{b}^\dagger)(\hat{c} + \hat{c}^\dagger),$$

$$\text{(D11)}$$

where g_3 denotes the coupling strength of the three modes with resonant frequencies $\omega_{a,b,c}$. We introduce an interaction picture with respect to the free Hamiltonian and obtain

$$\hat{\mathcal{H}} = g_3(\hat{a}e^{-i\omega_a t} + \hat{a}^\dagger e^{+i\omega_a t})(\hat{b}e^{-i\omega_b t} + \hat{b}^\dagger e^{+i\omega_b t})$$
$$\times (\hat{c}e^{-i\omega_c t} + \hat{c}^\dagger e^{+i\omega_c t}). \tag{D12}$$

Each of the modes is externally driven via an off-resonant pump; the corresponding driving frequencies are $\omega_{P,n}, (n \in a,b,c)$. In the next step we perform a displacement transformation of the form

$$\hat{a} = \bar{a}e^{-i(\omega_{P,a}-\omega_a)t-i\phi_a} + \hat{d}_1,$$
$$\hat{b} = \bar{b}e^{-i(\omega_{P,b}-\omega_b)t-i\phi_b} + \hat{d}_2, \tag{D13}$$
$$\hat{c} = \bar{c}e^{-i(\omega_{P,c}-\omega_c)t-i\phi_c} + \hat{d}_3,$$

where we keep the amplitudes $\bar{a}, \bar{b}$, and $\bar{c}$ real and introduce the pump phases ϕ_n. The first terms describe the strong-field component resulting from the external driving. Note, in this rotated frame we have to subtract the modes' resonant frequency from the pump frequency. We assume strong driving and thus neglect possible fluctuations at the pump frequencies; i.e., we make a stiff pump approximation. The second terms describe the field/fluctuations at the modes' resonant frequencies. After some algebra we find for the resonant interactions

$$\hat{\mathcal{H}} = g_3\bar{c}[\hat{d}_1^\dagger \hat{d}_2^\dagger e^{-i[\omega_{P,c}-(\omega_a+\omega_b)]t-i\phi_c}$$
$$+ \hat{d}_1^\dagger \hat{d}_2 e^{-i(\omega_{P,c}-(\omega_a-\omega_b))t-i\phi_c}]$$

$$+ g_3\bar{b}[\hat{d}_1^\dagger \hat{d}_3^\dagger e^{-i[\omega_{P,b}-(\omega_a+\omega_c)]t-i\phi_b}$$
$$+ \hat{d}_1^\dagger \hat{d}_3 e^{-i(\omega_{P,b}-(\omega_a-\omega_c))t-i\phi_b}]$$
$$+ g_3\bar{a}[\hat{d}_2^\dagger \hat{d}_3^\dagger e^{-i[\omega_{P,a}-(\omega_b+\omega_c)]t-i\phi_a}$$
$$+ \hat{d}_2^\dagger \hat{d}_3 e^{-i[\omega_{P,a}-(\omega_b-\omega_c)]t-i\phi_a}] + \text{H.c.} \tag{D14}$$

Here we made a rotating wave approximation. The choice of the pump frequencies determines the resonant interactions between two modes. Pumping at the sum of the frequencies results in nondegenerate parametric amplification, i.e., the first terms in the upper Hamiltonian. The second terms describe frequency conversion and are realized if one drives at the frequency difference of two modes. The latter would correspond to choosing the pumping scheme

$$\omega_{P,a} = \omega_b - \omega_c, \quad \omega_{P,b} = \omega_a - \omega_c, \quad \omega_{P,c} = \omega_a - \omega_b, \tag{D15}$$

which results in the effective Hamiltonian

$$\hat{\mathcal{H}}_{\text{int}} = G_c\hat{d}_1^\dagger \hat{d}_2 e^{-i\phi_c} + G_b\hat{d}_1^\dagger \hat{d}_3 e^{-i\phi_b} + G_a\hat{d}_2^\dagger \hat{d}_3 e^{-i\phi_a} + \text{H.c.}, \tag{D16}$$

with $G_n \equiv g_3\bar{n}$; here we again neglected counter-rotating terms. This is exactly the Hamiltonian for our building block. A basic gauge transformation yields Eq. (1) of the main text. Here one of the modes can be considered as the link oscillator which realizes the dissipative interaction between the remaining two modes. We note that one could as well employ a SQUID as the coupling element between the three modes as demonstrated recently [18].

[1] K. Fang, Z. Yu, and S. Fan, Realizing effective magnetic field for photons by controlling the phase of dynamic modulation, Nat. Photonics **6**, 782 (2012).

[2] J. Koch, A. A. Houck, K. L. Hur, and S. M. Girvin, Time-reversal-symmetry breaking in circuit-QED-based photon lattices, Phys. Rev. A **82**, 043811 (2010).

[3] A. Nunnenkamp, J. Koch, and S. M. Girvin, Synthetic gauge fields and homodyne transmission in Jaynes-Cummings lattices, New J. Phys. **13**, 095008 (2011).

[4] F. Mei, J.-B. You, W. Nie, R. Fazio, S.-L. Zhu, and L. C. Kwek, Simulation and detection of photonic Chern insulators in a one-dimensional circuit-QED lattice, Phys. Rev. A **92**, 041805 (2015).

[5] J. Ningyuan, C. Owens, A. Sommer, D. Schuster, and J. Simon, Time- and Site-Resolved Dynamics in a Topological Circuit, Phys. Rev. X **5**, 021031 (2015).

[6] W. Hu, J. C. Pillay, K. Wu, M. Pasek, P. P. Shum, and Y. D. Chong, Measurement of a Topological Edge Invariant in a Microwave Network, Phys. Rev. X **5**, 011012 (2015).

[7] Z. Lin, H. Ramezani, T. Eichelkraut, T. Kottos, H. Cao, and D. N. Christodoulides, Unidirectional Invisibility Induced by $\mathcal{PT}$-Symmetric Periodic Structures, Phys. Rev. Lett. **106**, 213901 (2011).

[8] S. Longhi, Invisibility in $\mathcal{PT}$-symmetric complex crystals, J. Phys. A: Math. Theor. **44**, 485302 (2011).

[9] N. Bender, S. Factor, J. D. Bodyfelt, H. Ramezani, D. N. Christodoulides, F. M. Ellis, and T. Kottos, Observation of Asymmetric Transport in Structures with Active Nonlinearities, Phys. Rev. Lett. **110**, 234101 (2013).

[10] L. Chang, X. Jiang, S. Hua, C. Yang, J. Wen, L. Jiang, G. Li, G. Wang, and M. Xiao, Parity-time symmetry and variable optical isolation in active-passive-coupled microresonators, Nat. Photonics **8**, 524 (2014).

[11] B. Peng, Ş. K. Özdemir, M. Liertzer, W. Chen, J. Kramer, H. Yilmaz, J. Wiersig, S. Rotter, and L. Yang, Chiral modes and directional lasing at exceptional points, Proc. Natl. Acad. Sci. USA **113**, 6845 (2016).

[12] A. Metelmann and A. A. Clerk, Nonreciprocal Photon Transmission and Amplification via Reservoir Engineering, Phys. Rev. X **5**, 021025 (2015).

[13] A. Metelmann and A. A. Clerk, Nonreciprocal quantum interactions and devices via autonomous feedforward, Phys. Rev. A **95**, 013837 (2017).

[14] P. Roushan, C. Neill, A. Megrant, Y. Chen, R. Babbush, R. Barends, B. Campbell, Z. Chen, B. Chiaro, A. Dunsworth et al., Chiral ground-state currents of interacting photons in a synthetic magnetic field, Nat. Phys. **13**, 146 (2017).

[15] L. Ranzani and J. Aumentado, Graph-based analysis of nonreciprocity in coupled-mode systems, New J. Phys. **17**, 023024 (2015).

[16] K. M. Sliwa, M. Hatridge, A. Narla, S. Shankar, L. Frunzio, R. J. Schoelkopf, and M. H. Devoret, Reconfigurable Josephson Circulator/Directional Amplifier, Phys. Rev. X **5**, 041020 (2015).

[17] K. Fang, J. Luo, A. Metelmann, M. H. Matheny, F. Marquardt, A. A. Clerk, and O. Painter, Generalized non-reciprocity in an optomechanical circuit via synthetic magnetism and reservoir engineering, Nat. Phys. **13**, 465 (2017).

[18] F. Lecocq, L. Ranzani, G. A. Peterson, K. Cicak, R. W. Simmonds, J. D. Teufel, and J. Aumentado, Nonreciprocal Microwave Signal Processing with a Field-Programmable Josephson Amplifier, Phys. Rev. Appl. **7**, 024028 (2017).

[19] G. A. Peterson, F. Lecocq, K. Cicak, R. W. Simmonds, J. Aumentado, and J. D. Teufel, Demonstration of Efficient Nonreciprocity in a Microwave Optomechanical Circuit, Phys. Rev. X **7**, 031001 (2017).

[20] N. R. Bernier, L. D. Tóth, A. Koottandavida, A. Nunnenkamp, A. K. Feofanov, and T. J. Kippenberg, Nonreciprocal reconfigurable microwave optomechanical circuit, Nat. Commun. **8**, 604 (2017).

[21] F. D. M. Haldane and S. Raghu, Possible Realization of Directional Optical Waveguides in Photonic Crystals with Broken Time-Reversal Symmetry, Phys. Rev. Lett. **100**, 013904 (2008).

[22] S. Raghu and F. D. M. Haldane, Analogs of quantum-Hall-effect edge states in photonic crystals, Phys. Rev. A **78**, 033834 (2008).

[23] M. Hafezi, E. A. Demler, M. D. Lukin, and J. M. Taylor, Robust optical delay lines with topological protection, Nat. Phys. **7**, 907 (2011).

[24] V. Yannopapas, Dirac points, topological edge modes and non-reciprocal transmission in one-dimensional metamaterial-based coupled-cavity arrays, Int. J. Mod. Phys. B **28**, 1441006 (2014).

[25] L. Lu, J. D. Joannopoulos, and M. Soljačić, Topological photonics, Nat. Photonics **8**, 821 (2014).

[26] V. Peano, C. Brendel, M. Schmidt, and F. Marquardt, Topological Phases of Sound and Light, Phys. Rev. X **5**, 031011 (2015).

[27] C. W. Gardiner and P. Zoller, *Quantum Noise* (Springer, Berlin, 2004).

[28] B. Peng, Ş. K. Özdemir, F. Lei, F. Monifi, M. Gianfreda, G. L. Long, S. Fan, F. Nori, C. M. Bender, and L. Yang, Parity-time-symmetric whispering-gallery microcavities, Nat. Phys. **10**, 394 (2014).

[29] M. Brandstetter, M. Liertzer, C. Deutsch, P. Klang, J. Schöberl, H. E. Türeci, G. Strasser, K. Unterrainer, and S. Rotter, Reversing the pump dependence of a laser at an exceptional point, Nat. Commun. **5**, 4034 (2014).

[30] H. Hodaei, M.-A. Miri, M. Heinrich, D. N. Christodoulides, and M. Khajavikhan, Parity-time–symmetric microring lasers, Science **346**, 975 (2014).

[31] A. Kamal and A. Metelmann, Minimal Models for Nonreciprocal Amplification Using Biharmonic Drives, Phys. Rev. Appl. **7**, 034031 (2017).

[32] Y. Chen, C. Neill, P. Roushan, N. Leung, M. Fang, R. Barends, J. Kelly, B. Campbell, Z. Chen, B. Chiaro *et al.*, Qubit Architecture with High Coherence and Fast Tunable Coupling, Phys. Rev. Lett. **113**, 220502 (2014).

[33] B. Abdo, A. Kamal, and M. Devoret, Nondegenerate three-wave mixing with the Josephson ring modulator, Phys. Rev. B **87**, 014508 (2013).

[34] T. Brecht, W. Pfaff, C. Wang, Y. Chu, L. Frunzio, M. H. Devoret, and R. J. Schoelkopf, Multilayer microwave integrated quantum circuits for scalable quantum computing, npj Quantum Information **2**, 16002 (2016).

[35] Z. K. Minev, K. Serniak, I. M. Pop, Z. Leghtas, K. Sliwa, M. Hatridge, L. Frunzio, R. J. Schoelkopf, and M. H. Devoret, Planar Multilayer Circuit Quantum Electrodynamics, Phys. Rev. Appl. **5**, 044021 (2016).

[36] B. Peropadre, D. Zueco, F. Wulschner, F. Deppe, A. Marx, R. Gross, and J. J. García-Ripoll, Tunable coupling engineering between superconducting resonators: From sidebands to effective gauge fields, Phys. Rev. B **87**, 134504 (2013).

[37] Y. Yin, Y. Chen, D. Sank, P. J. J. O'Malley, T. C. White, R. Barends, J. Kelly, E. Lucero, M. Mariantoni, A. Megrant *et al.*, Catch and Release of Microwave Photon States, Phys. Rev. Lett. **110**, 107001 (2013).

[38] M. Pierre, I.-M. Svensson, S. R. Sathyamoorthy, G. Johansson, and P. Delsing, Storage and on-demand release of microwaves using superconducting resonators with tunable coupling, Appl. Phys. Lett. **104**, 232604 (2014).

[39] D. Porras and J. J. García-Ripoll, Shaping an Itinerant Quantum Field into a Multimode Squeezed Vacuum by Dissipation, Phys. Rev. Lett. **108**, 043602 (2012).

[40] F. Beaudoin, M. P. da Silva, Z. Dutton, and A. Blais, First-order sidebands in circuit QED using qubit frequency modulation, Phys. Rev. A **86**, 022305 (2012).

[41] J. D. Strand, M. Ware, F. Beaudoin, T. A. Ohki, B. R. Johnson, A. Blais, and B. L. T. Plourde, First-order sideband transitions with flux-driven asymmetric transmon qubits, Phys. Rev. B **87**, 220505 (2013).

[42] C. Navarrete-Benlloch, J. J. García-Ripoll, and D. Porras, Inducing Nonclassical Lasing via Periodic Drivings in Circuit Quantum Electrodynamics, Phys. Rev. Lett. **113**, 193601 (2014).

[43] E. Flurin, N. Roch, J. D. Pillet, F. Mallet, and B. Huard, Superconducting Quantum Node for Entanglement and Storage of Microwave Radiation, Phys. Rev. Lett. **114**, 090503 (2015).